ABSTRACT

Title of Document: **SYNTHESIS AND CHARACTERIZATION OF SURFACTANT-FREE, FLUORESCENT POLY(LACTIC-CO-GLYCOLIC) ACID NANOPARTICLES TARGETED TO INTERCELLULAR ADHESION MOLECULE -1**

Zois Tsinas, Master of Science, 2014

Directed By: Associate Professor Silvia Muro,
Fischell Department of Bioengineering &
Institute for Bioscience and Biotechnology
Research

Targeted drug delivery to endothelial cells lining the vasculature can improve treatment of many pathologies. Intercellular adhesion molecule-1 (ICAM-1), a transmembrane glycoprotein overexpressed in many diseases, is a good determinant for endothelial targeting of drug nanoparticles (NPs). In this study we synthesized surfactant-free, FITC-labeled poly(lactic-co-glycolic) acid (PLGA) NPs coated with anti-ICAM, and used fluorescence microscopy and radiotracing to study their interaction with endothelial cells in culture and in vivo. These NPs were stable in storage conditions and degraded in conditions mimicking intracellular lysosomes. Furthermore, NPs showed specific ICAM-1 binding, which was enhanced in diseased-like conditions, followed by efficient uptake and lysosomal trafficking via

the CAM-mediated pathway. Intravenous administration of NPs in mice resulted in organ-specific accumulation, most prominently the lungs. Hence, surfactant-free, FITC-labeled anti-ICAM PLGA NPs enabled the study of NP interactions with biological systems, which along with their fast degradation profile in physiological-like conditions, will guide future therapeutic applications.

SYNTHESIS AND CHARACTERIZATION OF SURFACTANT-FREE, FLUORESCENT POLY(LACTIC-CO-GLYCOLIC) ACID NANOPARTICLES TARGETED TO INTERCELLULAR ADHESION MOLECULE -1

By

Zois Tsinas

Thesis submitted to the Faculty of the Graduate School of the
University of Maryland, College Park, in partial fulfillment
of the requirements for the degree of
Master of Science
2014

Advisory Committee:
Professor Silvia Muro, Fischell Department of Bioengineering & Institute for Biosciences and Biotechnology Research, University of Maryland, Chair
Professor Christopher Jewell, Fischell Department of Bioengineering, University of Maryland
Professor Peter Kofinas, Fischell Department of Bioengineering, University of Maryland

Table of Contents

List of Abbreviations

%ID.	Percentage of injected dose
%ID/g.	Percentage of injected dose per gram of tissue
αGal.	α-galactosidase
^{125}I.	125-Iodine
Anti-ICAM.	Antibody targeted to intercellular adhesion molecule-1
ASM.	Acid sphingomyelinase
BSA.	Bovine serum albumin
CAM.	Cellular adhesion molecule
cLABL.	Cyclo-(1,12)-PenITDGEATDSGC
DAPI.	4′,6-diamidino-2-phenylindole
DI water.	Deionized water
DLS.	Dynamic light scattering
EC.	Endothelial cell
EDC.	1-Ethyl-3-(3-dimethylaminopropyl) carbodiimide
ERT.	Enzyme replacement therapy
FITC.	Fluorescein isothiocyanate
GAA.	α-glucosidase
GPC.	Gel permeation chromatography
HUVEC.	Human umbilical vein endothelial cell
ICAM-1.	Intercellular adhesion molecule-1
IgG.	Immunoglobin G
LR.	Localization ratio
LSD.	Lysosomal storage disease
M6PR.	Mannose-6-phosphate receptor
MDC.	Monodansylcadaverine
Mw.	Weight average molecular weight
NP.	Nanoparticle

PBS……..	Phosphate-buffered saline
PDI……..	Polydispersity index
PCL……..	Poly(caprolactone)
PEG……..	Poly(ethylene glycol)
PEI……	Poly(ethyleneimine)
PGA……..	Poly(glycolic acid)
PLA……..	Poly(lactic acid)
PLGA……..	Poly(lactic-co-glycolic acid)
RES……..	Reticuloendothelial system
SEM……..	Scanning electron microscope
SI……..	Specificity index
TCA……..	Trichloroacetic acid
THF……..	Tetrahydrofuran
TNFα……	Tumor necrosis factor alpha

Section 1: Introduction and Background

1.1. Drug delivery systems

Drug delivery is the process of administrating pharmaceutical compounds and molecules to achieve therapeutic effect in humans. In order to improve the delivery of these agents, researchers have focused their studies on developing novel drug delivery systems, including micro- and nano-particles, transdermal patches, inhalers, drug reservoir implants, antibody-drug conjugates, etc. [1]. Nanoscale drug carriers can improve the delivery of therapeutic agents by controlling solubility, bioavailability, circulation time, biodistribution, and can provide controlled release [2-4]. Moreover, in comparison to micron-sized delivery carriers, nanocarriers have a unique ability to overcome some biological barriers and can be used for oral, intravenous, and inhalation form applications [5-8]. Their geometry, surface features, and other characteristics can vary according to the material they are derived from and the application intended. There are three major categories of materials that can be used to produce nanoscale drug carriers: a) biomolecules, such as lipids, DNA, proteins, and polysaccharides b) organic synthetic materials, such as carbon structures and polymers, and c) inorganic synthetic materials, such as metals [9-12]. These materials can be used to produce metal particles, quantum dots, carbon nanotubes, liposomes, micelles, dendrimers, and nanoparticles [4, 6, 9, 10, 13-16]. For decades, polymeric drug delivery systems fabricated with synthetic, natural, or hybrid polymers have

been widely used in the research arena due to the wide variety of structures that can be achieved. It is relatively easy to control their size and shape and produce solid, porous or hollow nanoparticles (NPs), polymeric micelles, polymersomes, and polymeric dendrimers (Figure 1) [15, 17-19]. All these different structures help to modulate the stability of drugs or biological agents, and offer useful controlled release properties [18, 20-22].

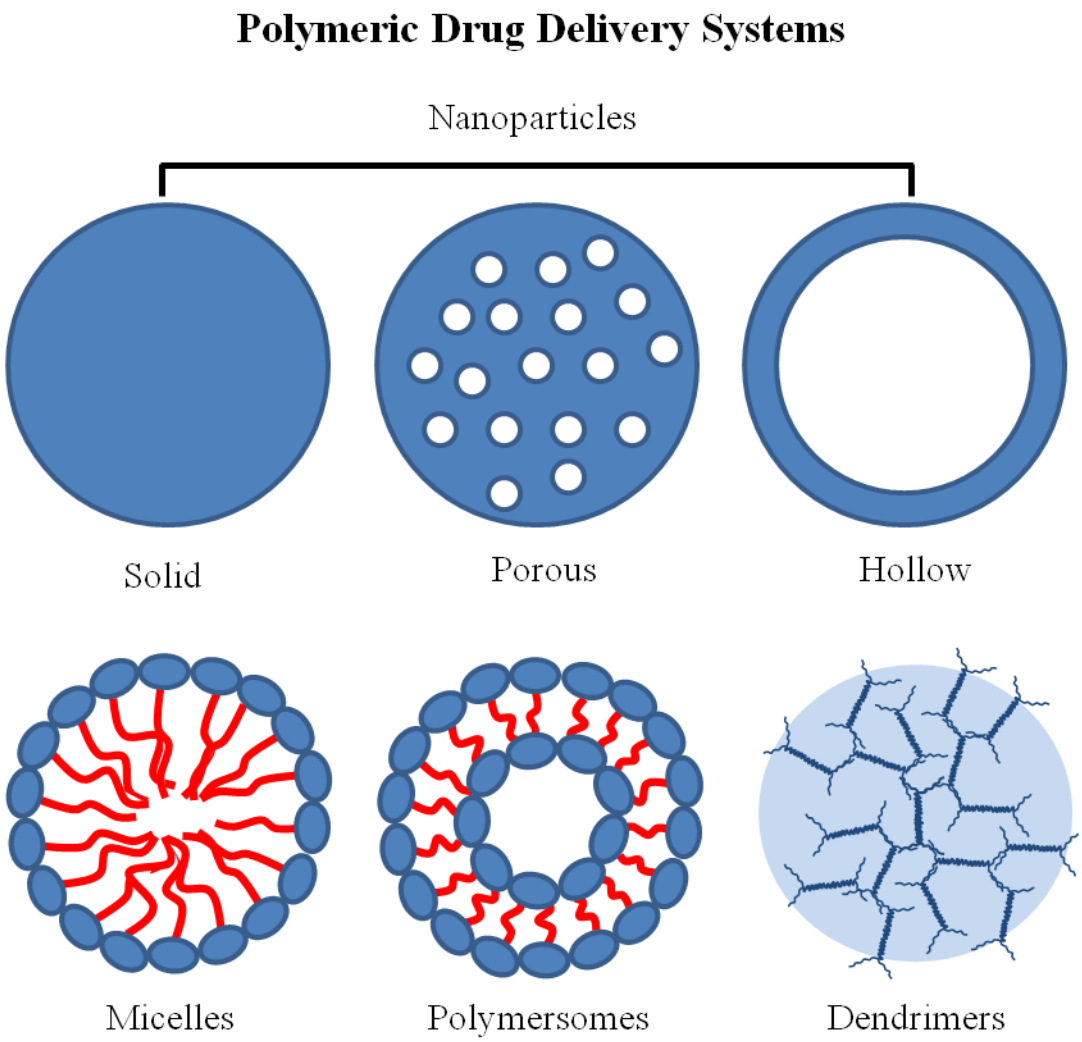

Figure 1. Various types of polymeric drug delivery systems currently exist. They can provide enhanced therapeutic efficacy due to their ability to prolong circulation, specific binding, and controlled release of cargo.

Polymeric NPs in particular can be easily produced from various types of inexpensive synthetic polymers such as polyanhydrides, poly(caprolactone) (PCL), poly(ethyleneimine) (PEI), poly(lactic acid) (PLA), poly(glycolic acid) (PGA), poly(lactic-co-glycolic acid) (PLGA), poly(ethylene glycol) (PEG), and poly(vinyl alcohol) (PVA), most of which are minimally toxic and biocompatible [18, 23-25]. This makes polymeric NPs highly preferable as delivery systems against inorganic structures such as carbon nanotubes that seem to associate with risk of inflammation [26]. Furthermore, polymeric NPs offer some advantages over other non-toxic structures such as liposomes: although both delivery systems are largely non-toxic, polymeric NPs can increase drug stability, are less limited to low encapsulation efficiencies, and prevent rapid leakage of water-soluble drugs [5, 18]. Ultimately, polymeric NPs have been extensively used to improve and enhance delivery of a wide range of therapeutics, including chemotherapeutics, proteins and enzymes, nucleic acids, etc. [27-30]. Therefore, polymeric NPs have great potential in the drug delivery field.

1.2. PLGA-based nanoparticles

One of the most commonly used synthetic polymers in drug delivery is PLGA. PLGA is a biocompatible and biodegradable material, and its biodegradability can be controlled by altering the ratio of lactic acid and glycolic acid in the co-polymer chain. An increase in the glycolic acid content of the co-polymer results in a higher

number of ester bonds in the polymer chain, which consequently leads to faster degradation kinetics [31]. This is very advantageous in drug delivery not only because controlled release of therapeutics can be achieved by altering the polymer composition, but also because these NPs can be fully degraded via hydrolysis of the ester bonds in the main chain of the co-polymer, into lactic acid and glycolic acid, substances that are biocompatible and have minimal toxic side effects [19, 31]. Furthermore, PLGA-based devices and drug delivery systems have already been used in the clinics, they are FDA-approved, and have been proven to be largely biocompatible [19, 32, 33].

Several methods have been suggested to prepare biodegradable NPs from PLGA by dispersing the preformed polymer, including single emulsion/solvent evaporation, solvent diffusion/nanoprecipitation, double emulsification, slating out, dialysis, supercritical fluid technology, and layer-by-layer deposition [18, 34]. These techniques can produce nanospheres and nanocapsules (containing oil or water) of various sizes (10 nm to 1 μm in diameter) [18, 34]. The most advantageous technique to produce nanospheres is the nanoprecipitation method first developed by Fessi and co-workers [35]. This technique is simple, rapid, and easy to perform. The most important advantage of this method is that it enables the production of small nanoparticles (100 - 300 nm in diameter) with narrow unimodal distribution and it is highly reproducible. The method requires two solvents that are miscible, such as acetone and water. Ideally the polymer must dissolve in the first one (the solvent, also known as the organic phase), but not in the second (the non-solvent, also known as

the aqueous phase). The nanoparticle formation occurs by a rapid desolvation of the polymer when the polymer solution is added to the non-solvent system. At that point the polymer-containing solvent diffuses into the dispersing medium and the polymer precipitates into small nanoparticles. The formation is governed by interfacial turbulences that take place at the interface of the solvent and non-solvent and result from complex and cumulated phenomena such as flow, diffusion and surface tension variations. Surfactants are not always needed and toxic organic solvents are generally excluded from this procedure. The main parameters that control the size of NPs are the polymer concentration, the aqueous phase agitation rate, and the volume ratio of the aqueous to organic phase [34, 36, 37]. In addition, drug content has been shown to affect size in the case of drug loaded NPs [37]. PLGA NPs have been successfully loaded with therapeutic molecules such as cancer drugs, proteins, enzymes, as well as DNA [38-44]. Drugs can be either loaded on the surface or inside the NPs according to their nature and physical properties. Hydrophobic drugs, such as cancer therapeutics, can be easily incorporated in the hydrophobic polymer matrix [38, 39]. Hydrophilic molecules on the other hand, such as proteins, enzymes, and DNA, do not dissolve in polar solvents and do not get easily entrapped in the hydrophobic polymer, due to their hydrophilic nature [37]. In order to tackle this problem, researchers have developed techniques to create PLGA NPs with hydrophilic pockets to encapsulate hydrophilic drugs, such as double emulsions and two step nanoprecipitation methods [42, 45].

It has been observed in cell culture experiments, that PLGA nanoparticles can be internalized by cells through clathrin mediated endocytosis [46]. Also, some studies showed that these NPs following cellular internalization undergo surface charge reversal (from anionic due to the free carboxylic end-groups in neutral pH, to cationic) in the acidic pH of the endosomes. This has been observed, in some instances, to promote escape from endosomes via interaction of NPs with these vesicular membranes [46, 47].

After intravenous administration, PLGA NPs will first encounter endothelial cells of the vasculature as the first layer of cells that must be targeted in order to penetrate through and reach the tissue of interest in the parenchyma. However, the hydrophobic surface of these particles is often recognized by the reticulo-endothelial system (RES) in the body as foreign and the NPs are quickly eliminated from the bloodstream by the clearance organs, mainly the liver and the spleen [32]. This, along with adsorption of proteins present in the serum to the surface of the NPs, a process known as opsonization, which subsequently leads to attachment of the opsonized NPs to macrophages and ultimately to their phagocytosis, are two of the major challenges that NP-based drug delivery has to overcome [48]. Surface modification techniques can be applied to address these limitations, either by altering the surface charge of the NPs or by attaching molecules that can: a) hide the hydrophobicity of the NP surface, b) target NPs to cell surface receptors to increase selective cellular binding and internalization through receptor-mediated endocytosis [48-52]. The most common molecule that can be used to provide a hydrophilic/non-fooling surface to the NPs is

poly(ethylene glycol) (PEG) [49]. This moiety has shown to prevent opsonization and increase NP circulation time, which occurs through steric repulsion and by blocking the electrostatic and hydrophobic interactions between the NP surface and the proteins present in serum [49]. Finally, as said, coating the surface of NPs with targeting ligands (such as antibodies or peptides) that recognize certain receptors on the surface of cells, can enhance binding specificity to selected cells and facilitate delivery to desired tissues reducing elimination by clearance organs [52-57].

1.3. Intercellular adhesion molecule-1 in drug delivery

A particularly interesting cell type in the development of targeted drug delivery systems are endothelial cells (ECs), which line the luminal surface of blood vessels. The endothelium is a specialized tissue that has a central role in inflammation, thrombosis, ischemia, and vascular oxidative stress, metabolic, and many other diseases. Therefore, targeting NPs loaded with therapeutics and intravenously administered to ECs may improve delivery to, into, or across ECs, in order to localize effects in the vascular lumen, desired intracellular compartments of the endothelium, or the sub-endothelial tissue space [58]. A molecule of interest for EC targeting is intercellular adhesion molecule-1 (ICAM-1), a transmembrane glycoprotein highly expressed on cells under stress or pathology, specially ECs [59].

ICAM-1 was first identified in 1986 by Springer and co-workers [60]. It is an immunoglobulin (Ig)-like transmembrane glycoprotein primarily expressed on ECs,

but also other cell types such as fibroblasts, epithelial cells, neurons, and tumor cells, and is upregulated by cytokines and proinflammatory factors [61, 62]. It is overexpressed during pathology in light of its role in leukocyte binding and transmigration during inflammation, making it a useful tool for targeting sites of disease in several organs and potentially assisting the transport of drug carriers from circulation to the inflamed tissue [59, 62].

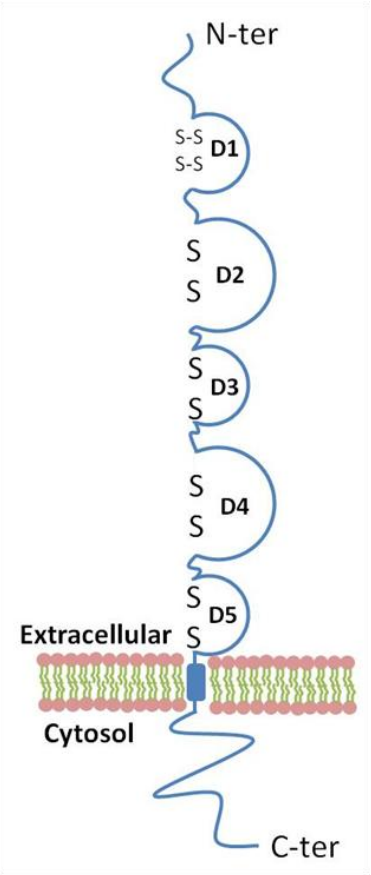

Figure 2. Intercellular adhesion molecule-1 structure.

ICAM-1 contains five Ig-like domains, a transmembrane domain, and a cytoplasmic tail (Figure 2). The cytoplasmic tail of the molecule has been shown to interact with the cytoskeleton-binding protein α-actin and this is likely what determines the cell surface distribution of ICAM-1 and its recruitment to points of interaction with leukocytes [62, 63]. ICAM-1 binds to two integrins belonging to the β_2 subfamily, expressed by leukocytes, as well as to CD43 receptor which is highly expressed by leukocytes and platelets. It also serves as an anchor for soluble fibrinogen and for the extracellular matrix factor hyaluronan [62]. The Ig-like domains of the ICAM-1 responsible for the binding of the molecule to the aforementioned ligands are mostly the first and the third domain [62]. Furthermore, it is proven that there are several different epitopes in

these two Ig-like domains of ICAM-1 that allow for binding of more than one ligand simultaneously [62, 64].

Moieties with affinity to ICAM-1, including peptides, antibodies, and antibody fragments have been explored as targeting agents in cell cultures, animal models, and humans for diagnostic methods, to suppress immunogenicity of transplanted organs or grafts, enhance cancer therapies, and to improve drug delivery for treatment of genetic diseases such as the lysosomal storage disorders (LSDs) [44, 64-69]. The important role of ICAM-1 in inflammation and its highly upregulated expression in diseased cells make it a very attractive target for delivery of drugs to diseased locations, particularly to the endothelium [70]. ICAM-1 is involved in endocytosis via a clathrin- and caveolar- independent pathway called cell adhesion molecule (CAM)-mediated endocytosis [59]. Previous work form our lab confirmed that anti-ICAM polystyrene NPs can bind to ICAM-1 on various human cell types such as ECs, fibroblasts, astrocytes, brain vascular pericytes, neurons, and gastrointestinal epithelial cells at a significantly greater extent than their non-targeted counterparts, particularly in diseased-like conditions [64, 71-74]. In addition, ICAM-1 targeted NPs of various sizes (100 nm to 5 μm in diameter) and shapes (spherical versus disk-shaped) have been shown to provide targeting and cellular uptake through CAM-mediated endocytosis, although small spherical NPs are endocytosed somewhat faster than larger and/or non-spherical counterparts [75, 76]. Furthermore, varying the density of anti-ICAM on the surface of the NPs has shown to modulate cell binding in

cell cultures and in vivo (in mice), indicating specific targeting and different biodistribution profile versus non-targeted NPs [71].

With regard to CAM-mediated endocytosis, it provides an alternative endocytic pathway independent of the classical caveolae- and clathrin-mediated pathways, as it involves signaling cascades similar to those observed when leukocytes bind to ICAM-1 [62]. This endocytic pathway is shown to traffic anti-ICAM NPs to lysosomes [59], which is a requirement for the treatment of LSDs, where recombinant enzymes need to be delivered to lysosomes within the diseased cells. Common endocytic pathways, such as clathrin-mediated endocytosis resulting from binding to mannose-6-phosphate receptor (M6PR), are not optimal for enzyme replacement therapy (ERT) of LSDs. M6PR, currently used in ERT, exists on most mammalian cells and its expression does not correlate to the homeostasis state of the cell. Also, its expression is not uniform in all cells and shifts with age. Ultimately, clathrin-mediated endocytosis has been observed to be disrupted in several LSDs, thus making M6PR less suitable for their effective treatment [77-80]. Our group has conducted several studies in cell cultures and mouse models that showed successful delivery of various lysosomal enzymes via the CAM route, including acid sphingomyelinase (ASM), α-galactosidase (α-Gal), and acid α-glucosidase (GAA) loaded on anti-ICAM NPs for the treatment of A-B Niemann-Pick, Fabry, and Pompe diseases, respectively [44, 52, 68, 75].

1.4. Targeting PLGA NPs to ICAM-1

Coupling antibodies to NPs can be generally achieved by one of the two following methods: a) covalent binding and b) physical adsorption [81]. Covalent attachment appears to be an effective way to permanently fix antibodies to nanocarriers, thus increasing the stability of the final product. In the case of PLGA NPs, 1-ethyl-3-(3-dimethylaminopropyl) carbodiimide (EDC) is used to chemically link the free carboxylic end groups located on the surface of PLGA NPs to the primary amine groups located on several amino acids on the antibody structure, forming a connecting amide bond [55, 82, 83]. However, this method usually fails to control the orientation of the antibody and affects negatively its activity since all conjugations through primary amines will involve amine groups, which may be located within the antigen-binding region [55, 81]. On the other hand, physical adsorption is usually achieved by mixing the nanocarrier solution with the antibodies for a certain amount of time, which allows for the protein to attach on the NP surface. Adsorption is governed by hydrophobic interactions between the antibodies, when at their isoelectric point (uncharged antibody molecules), and the surface of the NP. An advantage of this method is easiness of preparation, without the addition of any chemicals, while maintaining a high stability of coating even in the presence of serum [68]. It has also been speculated that this method benefits the correct orientation of the antibodies on the NP surface (hydrophobic interactions between the hydrophobic PLGA polymer and the hydrophobic part of the antibody molecules)

with the Fab' fragment accessible for binding to the specific antigen [55]. This method has been shown to produce immuno-nanoparticles that are able to efficiently target cells in vitro and in vivo [55].

PLGA NPs have been widely used by several research groups to target ICAM-1 [44, 56, 71, 84]. Peptides, such as Cyclo-(1,12)-PenITDGEATDSGC (cLABL), have been conjugated to PLGA NPs which showed specific binding and more rapid cellular uptake by ICAM-1-expressing lung epithelial cells, for potential enhanced lung cancer therapy [56]. Also, PLGA NPs conjugated with cLABL peptide demonstrated fast and specific binding to diseased-like human umbilical vein endothelial cells (HUVECs). Furthermore, these particles were internalized by the cells and trafficked to lysosomes to a greater extent than non-targeted PLGA counterparts [84]. In addition to these studies, our group has demonstrated that anti-ICAM PLGA NPs can significantly enhance binding to HUVECs over the non-targeted counterparts in cell culture and in vivo after intravenous administration in mice [71]. These NPs were specifically accumulated in the lungs, similar to model anti-ICAM polystyrene NPs [71]. Further studies have demonstrated that anti-ICAM PLGA NPs can be successfully coated with a therapeutic enzyme, ASM, enhancing the delivery of the enzyme in both wild-type, and A-B Niemann-Pick disease mouse models [44]. These findings highlight the potential for ICAM-1 targeting strategies in drug delivery.

Section 2: Significance and Innovation

Previous work with ICAM-1-targeted NPs, from our group, showed that they can efficiently target and deliver therapeutics in cell culture and in vivo, with promising results regarding the treatment of several LSDs [44, 52, 68, 85, 86]. Most of these studies were conducted using commercially available polystyrene NPs, which when targeted to ICAM-1 showed specific binding to diseased ECs and other cell types affected in LSDs, as well as efficient cellular uptake via a non-classical mechanism of endocytosis known as the CAM pathway with lysosomal trafficking [52, 59, 71, 87]. Furthermore, studies with ICAM-1-targeted PLGA NPs demonstrated that, similarly to the polystyrene NPs, this strategy can significantly enhance binding to ICAM-1 expressing cells and alter the biodistribution of therapeutics in mice versus their non-targeted counterparts [59, 71]. Ultimately, anti-ICAM PLGA NPs have shown to successfully deliver ASM in control and diseased mice [44]. Yet, prior to the work described in this study, the stability and degradation profile of anti-ICAM PLGA NPs in vitro, as well as their mechanism of uptake by ECs and their intracellular transport has not been characterized.

In order to study the above mentioned aspects, we formulated fluorescently labeled, surfactant free anti-ICAM PLGA NPs. The development of surfactant free PLGA NPs was pursued as opposed to previous formulations in the lab, in order to facilitate surface adsorption of targeting antibodies, reduce potential toxic effects, and obtain a fully biodegradable system from PLGA, which is FDA approved for

biological applications [19, 31, 32, 88]. In addition, another goal of this study was to incorporate fluorescent dyes, such as FITC, in the NPs structure in order to be able to visualize and characterize the trafficking of anti-ICAM PLGA NPs in cell culture via fluorescence microscopy. To our knowledge, this is the first time where FITC labeled, surfactant free PLGA NPs have been targeted to ICAM-1 and thoroughly studied as a drug delivery system in cell culture and in vivo. The results from this study not only will shed light into the stability, degradation, mechanism of uptake, and intracellular transport of these NPs, but will also portray the potential of using this drug delivery system to deliver therapeutics for treating diseases, such as LSDs.

Section 3: Methods

3.1. Materials

PLGA (50:50, DLG 3A; Mw=32kDa) was purchased from Evonic Industries (Germany). Monoclonal antibodies to ICAM-1, R6.5 (mouse anti-human-ICAM-1) and YN1 (rat anti-mouse-ICAM-1) were obtained from ATCC (Mananssas, VA). Non specific mouse or rat IgG, and secondary fluorescent antibodies were purchased from Jackson Immunoresearch (West Grove, PA). Radioisotope labeling with ^{125}Iodine was conducted using Na^{125}I from PerkinElmwe (Waltham, MA) and Iodogen pre-coated tubes from Thermo Fisher Scientific (Waltham, MA). Cell culture

media and related supplements were from Cellgro (Manassas, VA). All other reagents and solvents were from Sigma-Aldrich (St. Louis, MO).

3.2. PLGA NPs

3.2.1. Synthesis and characterization of PLGA NPs

PLGA NPs were synthesized using a 50:50 copolymer molar ratio with free carboxylic acid end groups and a Mw of 23 kDa. The polymer was first dissolved in acetone at a concentration of 20 mg/mL and a total volume of 25 mL to form the diffusing phase (organic phase). This phase was then added to filtered deionized (DI) water, which is the dispersing phase (200 mL), through a syringe positioned with the needle directly in the medium under moderate magnetic stirring (5,000 rpm, for 10 min). The formation of NPs was instantaneous and the solution was kept under mild agitation for 4 h to allow acetone to evaporate. Then, the NP solution was concentrated using a rotary evaporator by eliminating water and any residual solvent. Finally, NPs were stored at 4 ^{o}C. To formulate fluorescein isothiocyanate (FITC) loaded NPs, 5% wt/wt fluorescein was used in the diffusing phase. FITC was used as a marker into the NPs intended for cell culture experiments and visualization through fluorescence microscopy.

Particle size and polydispersity were determined by dynamic light scattering (DLS), and zeta potential was assessed by electrophoretic light scattering (Zetasizer nano-ZS90; Malvern Instruments; Westborough, MA). Each nanoparticle sample was

appropriately diluted in DI water ($1.37x10^7$ NPs/μL) prior to measuring ($n \geq 3$ per NP batch).

The morphology of NPs (surface appearance and shape) was analyzed by scanning electron microscopy (SEM). Samples were finely spread over slabs and dried under vacuum. Then, the samples were coated in a cathodic evaporator with a fine gold layer and observed using a scanning electron microscope from JEOL (Tokyo, Japan).

3.2.2. Iodination of proteins

Radioisotope labeling of antibodies or enzymes with ^{125}Iodine was done by incubating ~20 μCi of $Na^{125}I$ from PerkinElmer (Waltham, MA) and Iodogen pre-coated tubes from Thermo Fisher Scientific (Waltham, MA) with 100 μL of 1 μg/μL protein for 5 minutes at 4 ^{o}C. Free, non-bound ^{125}I was removed from the iodinated protein mixture by centrifugation (1,000g for 4 min) in a 6 kDa cutoff gel size exclusion column (BioRad, Hercules, CA). Prior to filtering the iodinated protein, the column was inverted several times to thoroughly homogenize the gel, then washed with 2 mL of phosphate-buffered saline (PBS) and packed by centrifugation (1,000g for 1 min). The concentration of the eluted iodinated protein was determined with a Bradford assay compared to a known bovine serum albumin (BSA) standard. The amount of free ^{125}I remaining in the eluted iodinated sample was estimated by performing trichloroacetic acid (TCA) precipitation assay. This was achieved by

mixing 2 μL/mL of iodinated protein in PBS supplemented with 3% BSA and 0.2 mL of TCA to precipitate protein. After a 15 min incubation period at room temperature, TCA samples were centrifuged (2,755g for 5 min) and the supernatant was measured for ^{125}I content using a gamma counter (2470 Wizard2; PerkinElmer; Waltham, MA). From this, the percent of free ^{125}I was determined and subtracted to estimate the specific activity of the iodinated protein (CPM/μg).

3.2.3. Antibody adsorption onto PLGA NPs

Where indicated, PLGA NPs were further coated by adsorption (hydrophobic interactions), either with control non-specific IgG, anti-ICAM, or a mix of anti-ICAM and IgG (at various molar ratios of anti-ICAM to non-specific IgG: 75:25, 50:50, 25:75, and 12.5:87.5). Non-coated counterparts were separated by removing the supernatant after centrifugation (13.8g for 3 min). Coated NPs were resuspended in PBS supplemented with 1% BSA for cell culture experiments, and 0.35% BSA for mouse experiments, followed by gentle sonication to prevent aggregation (~25 pulses for 5 sec at ~22.5 μm amplitude, using a sonicator with a set output frequency of 22.5 kHz; Microson™ XL2000; Qsonica, LLC; Newtown, CT). The number of antibody molecules per NP was determined by using ^{125}I-labeled antibodies to coat NPs. The total ^{125}I remaining in the NP preparation was divided by the total number of NPs to calculate total CPM/NP. This value was then multiplied by the known specific activity of the iodinated protein (CPM/μg) to determine the total amount of protein

coated per NP. The diameter, PDI, and zeta potential of the coated NPs was measured via DLS.

3.2.4. PLGA NPs stability and degradation in vitro

The stability of PLGA NPs was evaluated under storage conditions (4 °C, in DI water) for a 30 days period, and the samples were analyzed through DLS for size, polydispersity index, and scattering counts. In addition, FITC release from PLGA NPs was determined in storage conditions (up to 1 month incubation) using a microplate spectrophotometer (SpectraMax) at 490 nm excitation and 520 nm emission.

The fluorescence intensity of FITC-labeled NPs was also evaluated at different pH conditions (neutral pH and acidic pH to mimic lysosomal environment) and at room temperature. The fluorescence of each sample was measured using a microplate spectrophotometer (excitation: 490 nm; emission: 520 nm), after 15 min of incubation into the following conditions: NPs in PBS at 7.4 pH, NPs in PBS titrated with HCL at pH 4.5, NPs transferred from pH 7.4 (15 min) to pH 4.5 (additional 15 min), NPs transferred from pH 4.5 (15 min) to pH 7.4 (additional 15 min).

To determine in vitro degradation of PLGA NPs, antibody coated and non-coated particles were incubated in pH 7.4 and pH 4.5 buffers (non-salted PBS) at 37 °C for various time intervals (1, 2, 7, and 14 days). Samples were collected at each time point and dried overnight. Tetrahydrofuran (THF) was then added per sample to

dissolve the dry polymer, resulting in a 3 mg/ml PLGA solution. These samples were processed using positive filtration through a Whatman 0.2 μm pore-size filter (polytetrafluoroethylene membrane; PTFE) from Thermo Fisher Scientific (Waltham, MA). The Mw of the PLGA polymer was determined through gel permeation chromatography (GPC), using polystyrene standards. Finally, the size, polydispersity index, NP counts, and fluorescence intensity of the particles were measured at each time point.

3.3. Cell culture

3.3.1. Specific binding of anti-ICAM PLGA NPs to cells

Healthy or diseased (overnight treatment with 10 ng/mL of tumor necrosis factor alpha (TNF-α)) human umbilical vein endothelial cells (HUVECs), were seeded onto glass coverslips. Then, FITC-labeled anti-ICAM PLGA NPs were added to the cells and incubated for 1 h at 37 °C. Formulations were: **1)** control non-specific IgG NPs, **2)** anti-ICAM NPs (100% targeting valency), **3)** 75:25 anti-ICAM to non-specific IgG NPs (75% targeting valency), and 50:50 anti-ICAM to non-specific IgG NPs (50% targeting valency). The concentration of particles in all cases was $6.8x10^{10}$ NPs/mL. Cells were then washed three times with PBS to remove unbound NPs, fixed with cold 2% paraformaldahyde (PFA) for 15 min, and the nucleus stained with 14.3 μM blue 4′,6-diamidino-2-phenylindole (DAPI). Fluorescence images were captured with

SlideBook™ 4.2 software (Intelligent Imaging Innovations, Denver, CO) using an Olympus IX81 microscope (Olympus, Inc., Center Valley, PA), ORCA-ER camera (Hamamatsu, Bridgewater, NJ), a 60x objective (Olympus Uplan F LN; Olympus, Inc., Center Valley, PA) and DAPI, FITC, and/or Texas Red filters (1160A-OMF, 3540B-OMF, 4040B-OMF; Semrock, Inc., Rochester, NY). Images were analyzed using ImagePro 6.3 (Media Cybernetics, Silver Spring, MD) to estimate the total number of green fluorescent NPs associated per cell. Phase-contrast was used to determine the cell borders.

3.3.2. Endocytosis of anti-ICAM PLGA NPs

Healthy or diseased (TNF-α activated) cells were incubated at 37°C with the same FITC-labeled PLGA NP formulations described above, either continuously for 1, 3, 5, and 8 h, or for 1h pulse to allow NP binding, followed by washing to remove unbound NPs and replacement of fresh medium to continue incubation up to 3, 5, and 8 h (chase). Cells were then washed and fixed with 2% paraformaldehyde (PFA). Cell-surface bound NPs were counter-stained with 26.7 pM Texas Red goat anti-mouse secondary antibody. Since the fixed cells are not be permeabilized, the secondary antibody can only bind to anti-ICAM NPs on the cell surface and cannot reach NPs that are endocytosed into the cell. Fluorescence microscopy was used to visualize cell samples. In merged micrographs, green fluorescence alone revealed endocytosed NPs and yellow fluorescence (green + red) revealed surface-bound NPs.

Nuclei were stained with 14.3 μM DAPI (blue). From this, the total number of NPs endocytosed per cell can be estimated and compared to the total number of NPs associated per cell, to extrapolate internalization efficiency as percent internalization.

3.3.3. Internalization mechanism of anti-ICAM PLGA NPs

The mechanism by which cells endocytose anti-ICAM NPs was studied by performing similar experiments as those previously described, but in the presence of one of the following pharmacological inhibitors of endocytic transport: 3 mM amiloride (which inhibits CAM-pathway), 1 μg/mL filipin (which inhibits caveolae-mediated pathways), or 50 μM monodansylcadaverine (MDC; which inhibits clathrin-mediated pathways) [59]. The cells were pre-incubated with each inhibitor for 30 min at 37°C, and then NPs were added to the cells under the presence of the inhibitors. The effects of these inhibitors on the uptake of NPs were evaluated similarly as stated above, using fluorescence microscopy to calculate the internalization efficiency in each condition and compared to that of the control (incubation in absence of an inhibitor).

3.3.4. Lysosomal trafficking of anti-ICAM PLGA NPs

Lysosomes were labeled by incubating cells with 100 μM Texas Red dextran (10 kDa) for 45 min at 37°C to allow for dextran uptake, followed by removal of the

medium containing this marker. Incubation was then continued with fresh medium for a total of 45 additional min at 37°C to ensure trafficking of internalized dextran to lysosomes, as previously described [63]. Since dextran is a polysaccharide that cannot be enzymatically degraded in mammalian cells, it accumulates in lysosomes and allows for their visualization [64]. Cells were then incubated with the anti-ICAM PLGA NP formulations stated above for 1 h at 37°C to allow for binding. The cells were washed three times with PBS to remove unbound NPs, followed by replacement with fresh medium and additional incubation for a total of 3, 5, or 8 h at 37°C. Cells were fixed with 2% PFA and the nucleus stained with DAPI. The number of NPs that co-localized with Texas Red dextran-labeled lysosomes were measured using fluorescence microscopy. Green fluorescence alone represents cell associated NPs that did not co-localize with lysosomes, red fluorescence alone represents lysosomes without NPs, and yellow fluorescence (green + red) represents NPs localized to labeled lysosomes. From this, the total number of NPs co-localized with lysosomes could be estimated for each cell and compared to the total number of NPs associated per cell in order to extrapolate lysosomal trafficking efficiency as percent NPs co-localized with lysosomes.

3.4. In vivo studies

3.4.1 Circulation and biodistribution of anti-ICAM PLGA NPs in mice

NP circulation and biodistribution patterns in vivo were studied in wild type C57BL/6 mice (Jackson Laboratory; Bar Harbor, ME), anesthetized with an intraperitoneal (i.p.) injection (using a 28G hypodermic needle) of a 100 mg ketamine/10 mg xylazine/kg body weight buffered in 250 μL PBS. Anesthetized mice were then injected with $1.36x10^{12}$ NPs/kg body weight of control ^{125}I-IgG NPs versus anti-ICAM NPs (anti-ICAM formulations carried 100%, 50%, 25%, and 12.5% targeting valencies). Blood samples were collected by retro-orbital bleeds at 1, 15, and 30 min post-injection. After 30 min, mice were euthanized by cervical dislocation under anesthesia and tissues (brain, heart, kidneys liver, lungs, and spleen) were collected. Tissues were weighed and measured for ^{125}I content using a gamma counter. The weight and ^{125}I content of each organ and blood sample were used to calculate the following parameters: the percentage of injected dose (%ID), the percentage of injected dose per gram of tissue (%ID/g) to compare among organs of different size, the localization ratio to compare tissue-to-blood distribution (LR; %ID/g organ : %ID/g in blood), and the specificity index to compare targeted-to-non-targeted counterparts (SI; LR of anti-ICAM NPs : IgG NPs).

3.5 Statistics

All data are presented as mean ± standard error of the mean (S.E.M.). For statistical significance, size, PDI, number of counts, and zeta potential of NPs were calculated from ≥ 3 individual NP preparations, where ≥ 3 samples/NP preparation were measured three times. In vitro experiments including antibody coating efficiencies, NP stability, FITC release from NPs, and FITC fluorescence intensity in various pH conditions were conducted ≥ 2 times, and ≥ 3 samples per condition were analyzed. Cell culture experiments were performed in duplicates and were repeated ≥ 2 times. In vitro experiments were performed with ≥ 3 mice per condition. Statistical significance was determined as $p < 0.05$ by Student's t-test, for comparison between two groups, or Anova with post hoc Tukey's test, for comparison among > 2 groups.

Section 4: Results and Discussion

4.1. Synthesis and characterization of ICAM-1-targeted PLGA NPs

4.1.1. Introduction

Intravenous administration of therapeutics for intracellular delivery is receiving increasing attention. However, this method faces several challenges due to the intrinsic properties of most therapeutics: low bioavailability, insufficient in vivo

stability, fast clearance from the circulation, insufficient delivery to the site of interest, poor cellular uptake, endosomal trapping, degradation, etc. [89, 90]. These problems can be avoided to some extent by the usage of targeted NPs as carriers for drug delivery, since they can carry and protect therapeutics, offer targeting, enhance absorption into selected tissues, and improve intracellular penetration and trafficking [32, 89, 91]. The goal of this study is to develop fluorescently labeled, surfactant free PLGA NPs that are targeted to ICAM-1 for an enhanced binding to ECs of the vasculature, uptake, and lysosomal trafficking via the CAM-pathway. FITC-labeled PLGA NPs will allow us, for the first time, to study in detail the interactions of these particles with cells. Moreover, the elimination of surfactant from the formulation may offer a better surface for antibody adsorption, and might decrease toxic side effects as observed in the literature [88]. In this first part of the study we evaluated the size, the distribution, and the surface charge of PLGA NPs (plane, and FITC-loaded). Ultimately, we characterized their coating efficiency with anti-ICAM molecules and we evaluated stability in various conditions.

4.1.2. Synthesis of PLGA NPs

Nanoparticles were prepared from preformed PLGA polymer (50:50; Mw = 32 kDa) containing free carboxylic end groups, using the nanoprecipitation technique developed by Fessi and co-workers [35], but slightly modified to eliminate the usage of surfactants in the aqueous phase. The resulting nanoparticles had a mean diameter

of 166 nm, with a polydispersity index of 0.065. The mean zeta potential of the nanoparticles (measured in DI water) was -59 mV, indicating the presence of free carboxylic end groups of the polymer on their surface. Inclusion of fluorescein in the NP structure did not affect the aforementioned parameters. FITC-labeled NPs demonstrated a size of 186 nm in diameter with a polydispersity index of 0.066 and -55 mV zeta potential. Scanning electron microscopy images of non-labeled (Figure 3a) and FITC-labeled (Figure 3b) NPs revealed their regular spherical shape, as well as their unimodal distribution of size. FITC-loaded PLGA NPs were slightly deformed due to the higher magnification and their interaction with the electron beam (Figure 3b).

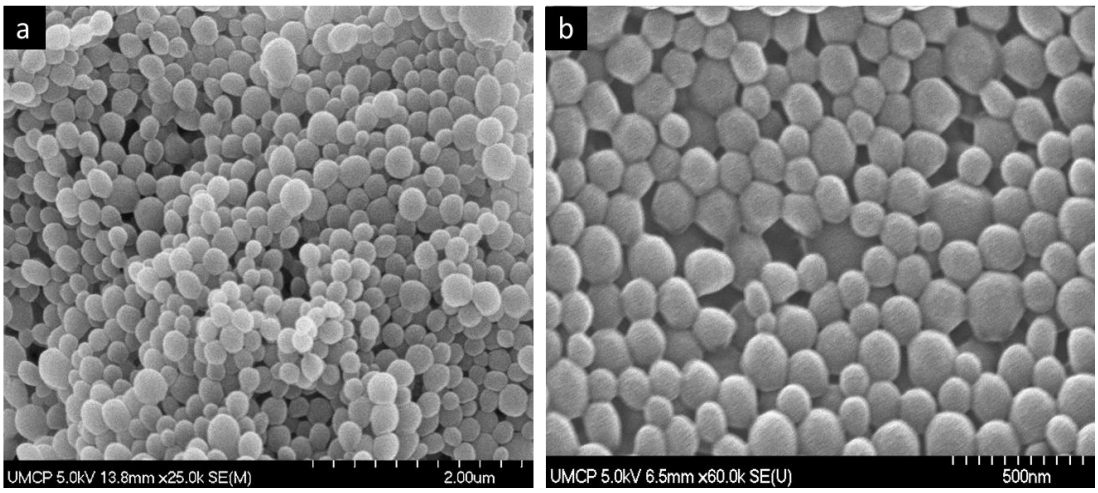

Figure 3. Scanning electron microscopy (SEM) images of (a) plane PLGA NPs, and (b) FITC loaded PLGA NPs.

4.1.3. Coating of anti-ICAM onto PLGA NPs

Targeting NPs to particular cell surface molecules for specific delivery of therapeutics to the site of interest is of great importance and has a wide spectrum of potential clinical applications, including drug, gene, and enzyme delivery [53, 92]. Our approach involves coupling anti-ICAM onto PLGA NPs for specific delivery of enzymes to diseased cells that over express ICAM-1 (e.g., lysosomal enzyme deficient cells, which our group pursues). Anti-ICAM PLGA NPs were produced via surface adsorption of antibodies onto the NP surface, due to hydrophobic interactions after mixing the two components together for an adequate amount of time (~1 h). To validate the presence of antibody coat on the surface of the NPs, antibody molecules were labeled with ^{125}I. As shown in Table 1, PLGA NPs fully coated with anti-ICAM (100% targeting valency) had a size of 266 nm in diameter, a PDI of 0.174, and carried 307 anti-ICAM molecules per NP. Furthermore, PLGA NPs containing fluorescein carried similar amount of anti-ICAM on their surface (312 anti-ICAM molecules per NP), which was also validated by an increase in their mean diameter (~40 nm in diameter increase) and polydispersity index versus the uncoated counterparts (PDI of 0.133 vs. 0.066 respectively). Also, the zeta potential of the coated nanoparticles was lower than that of the non-coated NPs in both FITC-loaded and non-loaded NP formulations (from -54.9 to -31.1 mV or 32.3 mV respectively). This validates the presence of antibody molecules on the surface of the NPs, since the surface charge of the coated particles is a result of the charged groups of the protein

that are present on the surface of the NPs and not the carboxylic end groups of the polymer, as in the case of the non-coated NPs.

Table 1. Characterization of PLGA NPs coated with antibodies.

	Size (nm)	Polydispersity Index	Zeta potential (mV)	Antibody Molecules/NP
Uncoated NPs	166.7±1.2	0.065±0.015	-59.4±0.6	N/A
100% IgG-NPs	273.9±5.2	0.204±0.006	-36.8±0.5	237.6±15.2
100% Anti-ICAM-NPs	266.4±4.8	0.174±0.016	-32.3±0.2	307.6±1.7
FITC uncoated NPs	186.4±3.3	0.066±0.014	-54.9±0.4	N/A
FITC 100% IgG-NPs	233.4±2.3	0.201±0.002	-29.3±0.1	215.7±9.2
FITC 100% anti-ICAM-NPs	227.3±2.1	0.133±0.012	-31.1±0.1	312.8±18.4

N/A = not applicable. Data shown are mean values ± S.E.M. ($n \geq 3$).

Furthermore, PLGA NPs coated with non-specific IgG exhibited similar characteristics and variations to the anti-ICAM-PLGA NPs: an increase in their mean diameter from 166.7 nm to 273.9 nm, and a decrease in their surface charge from -59.4 mV to -36.8 mV. However, non-specific IgG appeared to coat less efficiently on the surface of the particles, since IgG-NPs carried around 29% less antibody molecules than anti-ICAM NPs. This is probably due to the differences in the hydrophobic sequences and/or the isoelectric point of each antibody.

In this study we also investigated the role of antibody density on the surface of NPs. This parameter can help us optimize ICAM-1-driven endothelial targeting for therapeutic interventions using this targeting strategy for future applications [93]. To produce PLGA NPs with different anti-ICAM valencies we incubated the NPs with a mixture of non-specific IgG molecules and anti-ICAM molecules at different molar

ratios (25:75, 50:50, 75:25, and 87.5:12.5). As shown in Table 2, we were able to obtain different densities of anti-ICAM molecules coated on the surface of NPs by altering the molar ratio of these two antibodies, since 50%-valency anti-ICAM NPs carried 148 anti-ICAM molecules versus 100%-valency anti-ICAM NPs that carried 307 antibody molecules. Similar behavior was observed for the 25%- and 12.5%-valency formulations, where anti-ICAM molecules per NP were decreased by half (to 64 and 38 antibodies per NP, respectively).

Table 2. PLGA NPs coated with different valencies.

	Size (nm)	**Polydispersity Index**	**Zeta potential (mV)**	**Anti-ICAM-1 Molecules/NP**
Uncoated NPs	166.7±1.2	0.065±0.015	-59.4±0.6	N/A
Anti-ICAM NPs				
−100%-valency	266.4±9.8	0.174±0.016	-32.3±0.2	307.6±1.7
−75%-valency	270.8±4.6	0.192±0.012	N/D	221.7±9.4
−50%-valency	*271.3±3.5	0.205±0.004	N/D	148.9±11.8
−25%-valency	*293.5±3.6	0.202±0.003	N/D	64.5±2.9
−12.5%-valency	*316.5±5.7	0.256±0.006	N/D	38.9±1.7

N/A = not applicable. N/D = not determined. Data shown are mean ± S.E.M. ($n \geq 3$).
*NPs are also coated with non-specific IgG to obtain a 100% coated surface.

On the other hand, the size of the coated nanoparticles was relatively similar between the 100%, 75%, 50%, and 25%-valency NPs, varying from 266.4±9.8 to 329.5±3.6 nm in diameter, since NPs were also coated with non-specific IgG to obtain a fully coated surface. However, as the number of anti-ICAM molecules decreases on the surface of the NPs we observed that NPs exhibited larger sizes, resulting to a difference of almost 50 nm in diameter among the 100% anti-ICAM NPs and the 12.5% counterpart.

4.1.4. PLGA NPs stability studies

The stability of the NPs is of major importance for the consistency of the cell culture and mice experiments. Therefore, short term size stability of the non-coated and non-FITC labeled NPs was evaluated at storage conditions (4 ^{o}C, in DI water). No increase in the size of NPs was observed for 30 days (Figure 4a), and their PDI was well below 0.2 at each time point (Figure 4b). This indicated that the nano-colloidal suspension remains stable in storage conditions for at least one month. Furthermore, the number of NP scattering counts measured by DLS were consistent over time (around 350 kcps), indicating that NPs do not degrade or precipitate during this time.

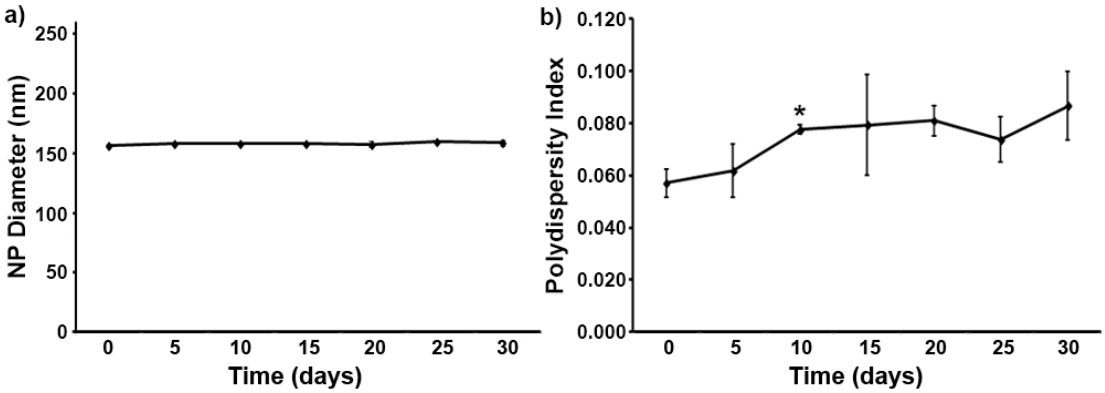

Figure 4. NP stability in storage conditions (deionized water, 4 ^{o}C). Data collected by dynamic light scattering. (a) Size of NPs over time (diameter in nm); (b) polydispersity index of NPs over time. *p≤0.05, compares each time point to day 0, by Student's t-test. Data are mean ± S.E.M. (n ≥ 3). Small errors in (a) are masked by symbols.

As previously mentioned, to study the interactions between NPs and cells in culture, we incorporated fluorescein as a marker into the NPs. Since fluorescein was physically entrapped in the polymer matrix during the NP formation and not

covalently attached to the polymer chain, we evaluated fluorescein release and fluorescence stability of NPs in the following scenarios: a) under storage conditions (deionized water, 4 ^{o}C) and b) in PBS at 37 ^{o}C, in either pH 7.4 or pH 4.5. To evaluate the fluorescence intensity of NPs under storage conditions, samples of NP solution were taken from the stock vial at various time intervals (day 0, day 7, day 20, and day 30). The particles were centrifuged (10 min at 12,000 g), the supernatant was then removed, and the fluorescence intensity of the pellet (consisting of NPs) and supernatant (containing free dye) were measured using a spectrophotometer (FITC excitation = 490; emission = 520). The results demonstrated that FITC loaded NPs retain the dye under storage conditions without showing any statistically significant release of FITC (Figure 5). These results, combined with the results from Figure 4, indicate that FITC-loaded PLGA NPs produced in this study can be stored at 4 ^{o}C in deionized water solution and maintain their fluorescence intensity, and size for at least 30 days.

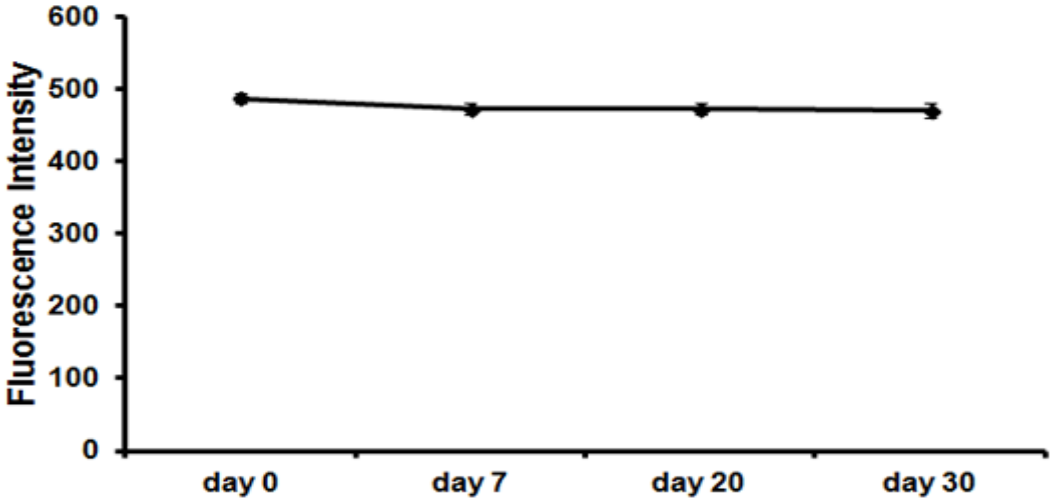

Figure 5. Fluorescence intensity of FITC loaded PLGA NPs at 4 ^{o}C, in deionized water. Changes in fluorescence intensity of NPs after removal of the supernatant, containing the free dye, at various time points. Data are mean ± S.E.M. ($n \geq 3$).

We also followed the stability of antibody coating on the surface of NPs during storage at 4 ^{o}C in 0.35% BSA-PBS (storage conditions). For this experiment we radiolabeled anti-ICAM-1 with ^{125}I and we quantified the number of antibody molecules per NP over time using a gamma counter. At each time point, NPs were centrifuged (13.8g for 3 min) and the radioactivity of the pellet (antibodies bound to NPs) and supernatant (released antibodies) were measured to determine the % release of antibodies over time. As shown in Figure 6, there is no statistical significance between the differences on the samples collected at 1 h, 3 h, 24 h, and 3 days compared to the initial coat (0 min). Therefore, particles had a fairly stable coat, with each particle carrying the same number of antibodies within 3 days under storage conditions.

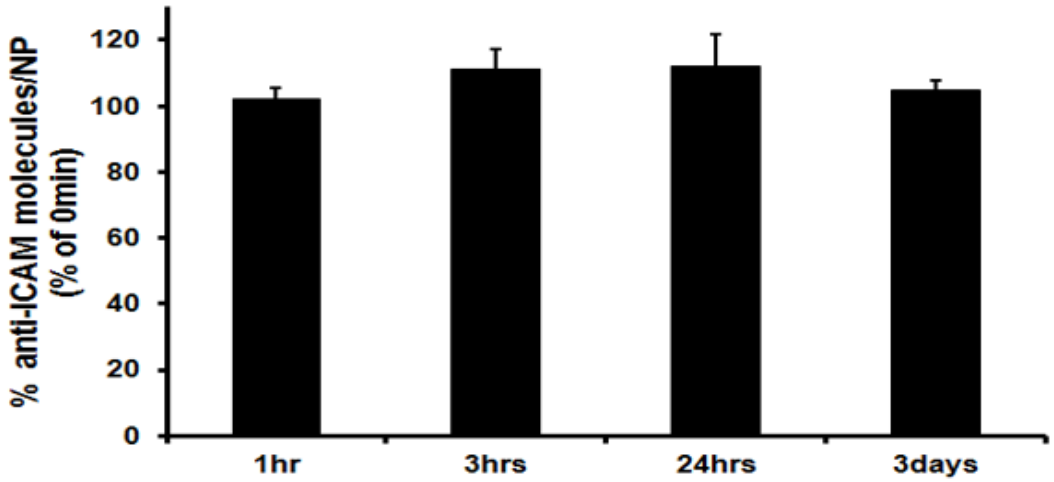

Figure 6. Coating stability of anti-ICAM-1 on the surface of PLGA NPs under storage conditions (0.35% BSA-PBS, 4 ^{o}C). Relative number of antibodies per NP at various time points after preparation (control, time = 0 min). Data are mean ± S.E.M. ($n \geq 3$).

Next, to mimic the pH conditions in circulation and the environment where NPs bind to cells, as well as the lysosomal pH conditions, NPs were incubated in PBS at pH 7.4 versus PBS at pH 4.5, respectively. First, NP samples were incubated for 15 min at 37 ^{o}C in PBS at pH 7.4 or 4.5, and their fluorescence intensity was measured by spectrophotometry using excitation and emission wavelengths of 490 and 520 nm (Figure 7). The results from this experiment showed that, as expected, FITC loaded PLGA NPs suffered a decay in fluorescence intensity when suspended in an acidic solution (pH 4.5) compared to NPs suspended at neutral pH. Then, NPs were transferred to neutral pH after 15 min incubation at pH 4.5, showing that the fluorescence intensity can be fully recovered, since there was no statistically significant change between these groups, whereas NPs transferred from neutral to acidic pH lost their fluorescence, exhibiting similar intensity to those in acidic

conditions. Hence, the change in intensity at pH 4.5 is due to reversible quenching, and not release of the dye from the NPs. This result is crucial because it enables us to trace these NPs inside certain compartments of the cells, such as lysosomes, where the pH is around 4.5, since the lysosomal pH is neutralized after cell fixation, allowing us to visualize NPs by fluorescence.

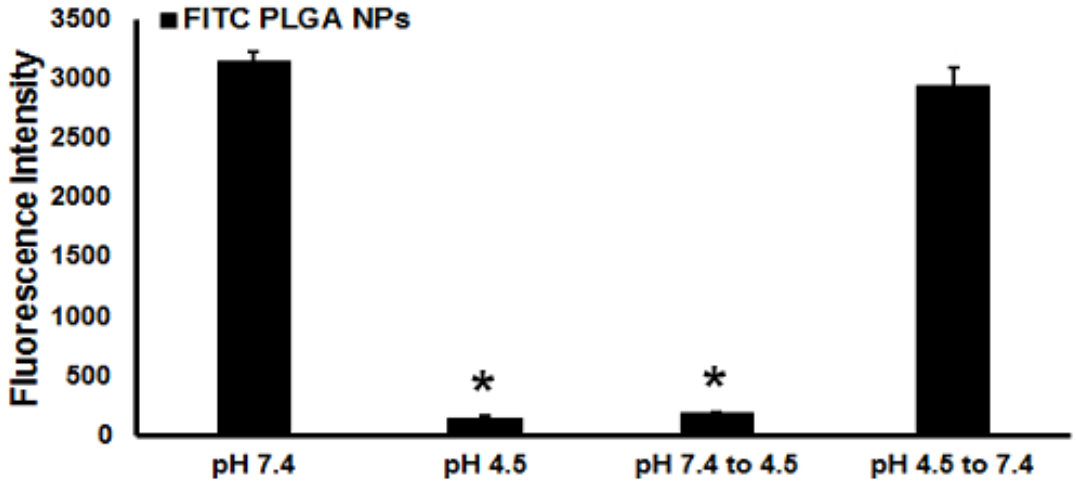

Figure 7. Fluorescence intensity of FITC loaded PLGA NPs at room temperature, in pH 7.4 and pH 4.5. *p≤0.05, compares the fluorescence intensity of NPs against standard incubation at 7.4 pH, by Student's t-test. Data are mean ± S.E.M. (n ≥ 3).

4.1.5. In vitro degradation of FITC loaded PLGA NPs

The degradation profile of PLGA NPs plays a crucial role in designing drug delivery systems that can transport drugs to the site of interest, control drug release, and ultimately allow degradation into products that can be easily cleared from the body without causing any major side effects or toxicity [94, 95]. In this study, we tested degradation of antibody-coated (using IgG as an example) versus non-coated FITC-

loaded PLGA NPs in vitro. NPs were incubated for 1, 2, 7, or 14 days at pH 7.4 or 4.5 and 37 ^{o}C. Samples from each condition were taken over time and processed to determine changes in the diameter of NPs, their scattering counts, the release of FITC from NPs, and the co-polymer (PLGA) molecular weight (Mw). With regard to the size of non-coated NPs, no significant changes were observed (Figure 8a) as their diameter remained constant, around 175 nm at pH 7.4 (Figure 8a, blue line). Also, non-coated NPs exhibited similar sizes over time at pH 4.5, with diameters around 190 nm (Figure 8a, red line). On the other hand, when incubated at pH 7.4 or 4.5, IgG-coated NPs seemed to experience a drop in their diameter at day 2 and 1, respectively, resulting in sizes similar to those of the non-coated NPs. This drop did not seem to be caused by NP degradation, since the average Mw of the co-polymer did not seem to change till day 2 (Figure 10). Instead, perhaps release of the antibody coating from the surface of the NPs might have caused this effect. IgG-coated NPs incubated at pH 4.5 lost their coat 1 day earlier than their counterparts at neutral pH, indicating that lysosomal-like pH has an effect on this phenomenon. Ultimately, the size of the coated NPs increased after the first drop is size, so that the NPs at both pH environments reached similar final sizes, around ~350 nm on day 14. This increase in size is probably attributed to aggregation of detached antibody molecules that may affect the nano-colloidal stability of the NPs. In that case, NPs might collide with each other forming aggregates of two or more NPs. Large aggregates could precipitate, while smaller aggregates could still remain in suspension, affecting the average size of the sample. A careful look at the size of the IgG-coated NPs at day 14

is indicative of the existence of dimers in the NP solution, since the average size of the sample is double the size of the non-coated NPs. However, this experiments was only conducted once and a more careful examination is needed.

Additionally, information collected from the scattering counts (kcps) of each NP sample (Figure 8b) revealed that non-coated NPs incubated at pH 7.4 had similar counts over time and along with their similar size, their concentration seem to remain constant. On the other hand, non-coated NPs incubated at pH 4.5 revealed a significant drop in the scattering counts between time 0 and day 14, indicating a loss in the number of NPs, which could be due to degradation or precipitation . IgG-coated NPs incubated at pH 4.5 behaved similarly, resulting in a decrease on the number of counts overtime, from 246 to 154 kcps. Finally, the IgG-coated NPs at pH 7.4 showed a small decrease in the kcps values, which is probably attributed to the aggregation of NPs in the sample due to the presence of free antibodies, in accord with the results obtained from the NP size measurements.

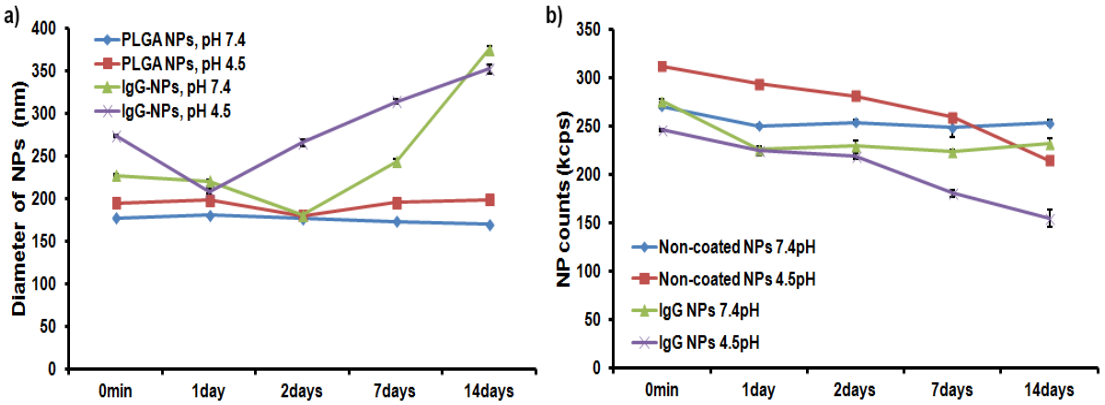

Figure 8. IgG-coated and non-coated FITC-PLGA NPs in pH 7.4 and 4.5, at 37 ^{o}C. (a) changes in the diameter (nm) of NPs over time; (b) changes in the number of counts (kcps) over time. Data are mean ± S.E.M. ($n \geq 3$).

In addition to these data, we also evaluated the release of FITC from the NPs, which is indicative of NP degradation, since FITC is physically entrapped in the polymer matrix. Our FITC stability studies in section 4.1.3 (Figure 5), showed that there is no significant release of FITC from the PLGA NPs under storage conditions for up to 30 days incubation. Therefore, an increase in the FITC release over time in any of the conditions tested in this study would be due to polymer degradation and escape of the dye from the NP matrix. Indeed, as shown in Figure 9, there is an increase in the percent of free dye between 0 min and day 14 for all the different formulations in every condition. Furthermore, as expected, NPs incubated at pH 4.5 exhibited higher FITC release than at pH 7.4, regardless of the presence of antibody on their surface. However, the differences in the % release of the dye between pH 7.4 and 4.5 in the case of IgG-coated NPs are significant only after day 7, compared to the non-coated NPs where significant differences were observed after day 2.

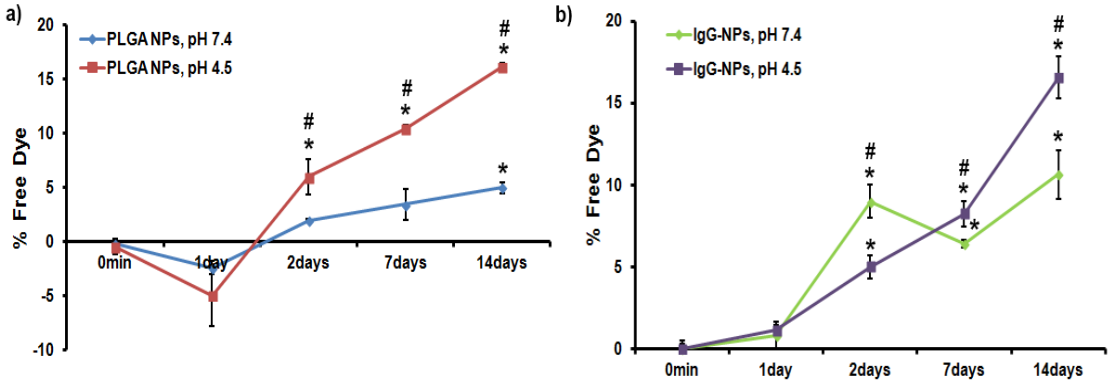

Figure 9. FITC release from IgG-coated PLGA NPs at physiological-like conditions. Percentage of free fluorescent dye in solution after incubation of non-coated and IgG-coated FITC PLGA NPs at 37 ^{o}C, and pH 7.4 or 4.5 for a period of 14 days. The amount of free dye in the initial prep was subtracted in order to account for release over time. (a) % free dye in the case of non-coated NPs over time; (b) Percent free dye in the case of IgG-coated NPs over time. *$p \leq 0.05$, compares each time point to the initial time (time = 0) for each condition, by Student's t-test; $^{\#}p \leq 0.05$, compares pH 7.4 to 4.5 for each condition, by Student's t-test. Data are mean ± S.E.M. ($n \geq 3$).

Finally, samples from each time point were analyzed by gel permeation chromatography (GPC), and the Mw of the PLGA co-polymer was determined. Figure 10 summarizes the results of the analysis for the different formulations at different conditions. In the case of non-coated NPs (Figure 10a and Figure 10b), where the polymer chain had an initial Mw around 23 kDa, degradation was observed at day 2 with a similar profile when comparing pH 7.4 versus 4.5 till that time. On day 7, the co-polymer Mw of NPs at pH 4.5 was 1 kDa lower that of the NPs in pH 7.4, while on day 14 NPs at pH 4.5 seemed to exhibit high degradation with a final Mw of 7.5 kDa (3 fold decrease). In the case of IgG-coated NPs (Figure 10c and Figure 10d), they exhibited a much faster degradation rate when incubated at pH 4.5 versus their counterparts at pH 7.4. Furthermore, it appears that PLGA NPs incubated at pH 4.5 had the same degradation rate regardless of the presence of antibody

coating. On the other hand, when particles were suspended at pH 7.4, there seemed to be less degradation associated with IgG-coated NPs versus non-coated counterparts. This suggests that antibody coating may protect the polymer from degrading at some extent.

All in all, the highest degradation was observed in the case of incubation at pH 4.5. Also, at low pH the degradation of the polymer was independent of the antibody coating. NPs at pH 7.4 still degrade over time, but at a slower pace and lower extent. Finally, at pH 7.4 antibody coating was more stable than at pH 4.5, and it may remain on the surface of the particles for longer periods of time somewhat protecting the polymer from degrading. These results pair well with the results obtained from the NP size data, the kcps values, and the FITC release described above.

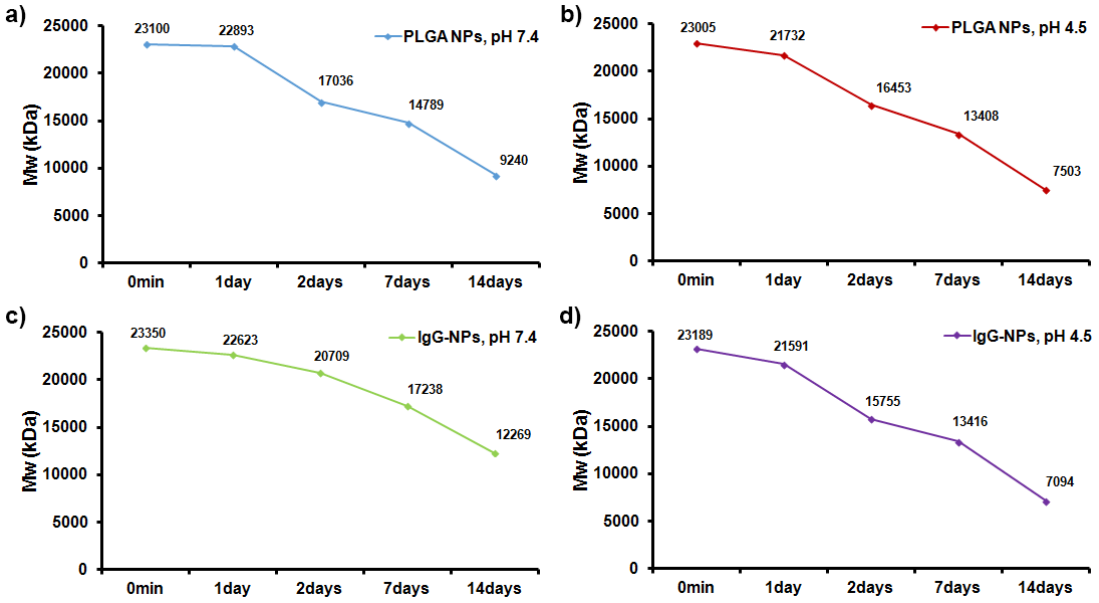

Figure 10. Changes in the Mw of PLGA polymer chains when IgG-coated and non-coated FITC-PLGA NPs were incubated at pH 7.4 and 4.5, at 37 ^{o}C for a period of 14 days. (a) Mw of PLGA polymer from non-coated PLGA NPs at pH 7.4; (b) Mw of PLGA polymer from non-coated PLGA NPs at pH 4.5; (c) Mw of PLGA polymer from IgG-coated PLGA NPs at pH 7.4; (d) Mw of PLGA polymer from IgG-coated PLGA NPs at pH 4.5.

4.2. ICAM-1-targeted PLGA NPs in cell cultures

4.2.1. Introduction

Targeted drug delivery aims to effective accumulation of NPs and their cargo within particular diseased tissues. After intravenous administration of NPs, binding and uptake of the NPs from the endothelial layer surrounding the blood vessels plays a crucial role for delivery of therapeutics to diseased ECs, while at the same time it allows for penetration and transport of NPs from the bloodstream into subjacent tissues [45]. Targeting NPs to ECs may also decrease non-specific clearance of drugs

from the bloodstream, allowing site-specific delivery and reducing side effects [96]. ICAM-1 is a molecule expressed on ECs, particularly those most severely altered by pathological conditions [70]. Targeting ICAM-1 can provide intracellular delivery of therapeutics to the endothelium, since ECs have previously shown to internalize anti-ICAM polystyrene, or PLGA NPs via a unique, newly defined pathway, known as CAM-mediated endocytosis [59, 71]. In this study, we used for the first time surfactant free, FITC-labeled PLGA NPs targeted to ICAM-1 in order to explore in detail the capacity of these NPs to target endothelial cells. Then, we studied in more detail the endothelial uptake of these NPs by testing parameters such as the antibody valency, the concentration of particles, the mechanism of internalization, and ultimately their intracellular trafficking.

4.2.2. Binding of anti-ICAM PLGA NPs to HUVECs

Binding of targeted PLGA NPs to ICAM-1 on tumor necrosis factor alpha (TNFα) stimulated HUVEC cells, to mimic a pathological condition, is a prerequisite for uptake and further intracellular as well as transcellular trafficking. Thus, we first tested the specificity and efficiency of ICAM-1-targeted PLGA NPs to bind on ECs. FITC-labeled NPs were coated with anti-ICAM to prepare anti-ICAM PLGA NPs, as described earlier. For this initial study we used anti-ICAM NPs bearing 100% valency and control IgG NPs, both with similar properties as shown in Table 1.

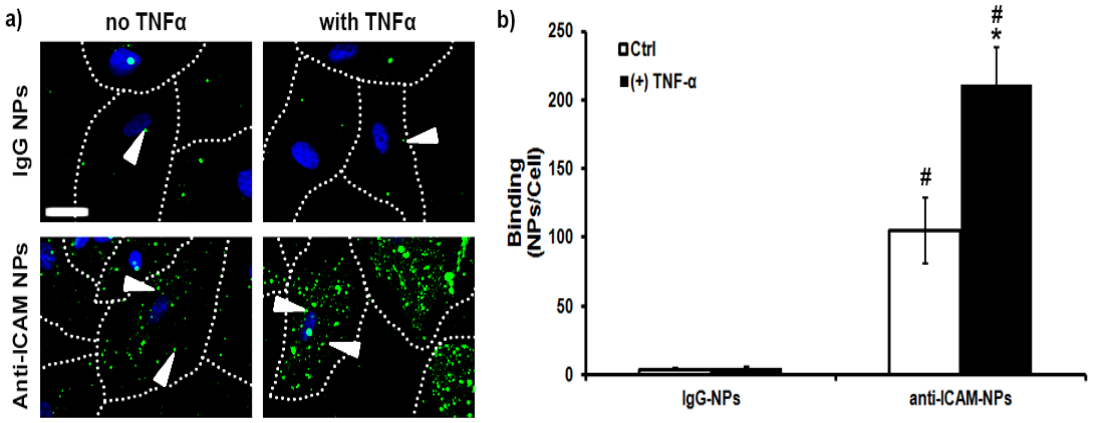

Figure 11. Binding of FITC anti-ICAM PLGA NPs to HUVECs. (a) Green FITC-labeled IgG or anti-ICAM PLGA NPs incubated with control or TNFα-treated HUVECS for 1 h at 37 ^{o}C (green NPs = arrowheads). Scale bar = 10 μm. Blue = nuclei of the cells. Dashed lines represent the cell borders, as observed by phase contrast. (b) Binding of NPs incubated with control or TNFα-activated cells for 1 h at 37 ^{o}C is shown. *p≤0.05, compares TNFα to control cells for each NP formulation; $^{\#}$p≤0.05, compares IgG NPs to anti-ICAM NPs, by Student's t-test. Data are mean ± S.E.M.

Fluorescence microscopy showed that FITC-labeled anti-ICAM PLGA NPs bound specifically to control endothelial cells: 105±24 NPs/cell versus 4±1 NPs/cell for non-specific IgG NPs (Figure 11). Also, in pathological-like conditions (TNF-α activated cells), binding of anti-ICAM NPs was significantly enhanced compared to control cells (211±27 NPs/cell; 2-fold enhancement), while IgG NPs showed no binding enhancement (Figure 11). This result is in agreement with the overexpression of ICAM-1 molecules on the cell membrane of cells in disease-like conditions, known from the literature [97].

In addition to these results, we also compared the binding behavior of anti-ICAM PLGA NPs coated with different anti-ICAM densities (100%, 75%, and 50% targeting valencies) to TNFα-activated HUVECs. As shown in Figure 12,

unexpectedly, there was no statistical significance between binding for these three different formulations: 211±27 NPs/cell for 100%-valency, 204±22 NPs/cell for 75%-valency, and 227±20 NPs/cell for 50%-valency. Previous data with polystyrene NPs have shown that NPs with higher anti-ICAM densities enhance binding over NPs with less number of antibodies on their surface [71]. However, for this to occur the number of antibody molecules per NP needs to be below a certain threshold. For this experiment 50% anti-ICAM NPs was the formulation with the lower antibody density tested, which resulted to ~159 antibodies/NP. It appears that NPs with more than 150 antibodies on their surface can effectively target diseased cells that overexpress ICAM-1 on their surface to the same extent within 1 h of incubation. If we were using NPs with a 25%-valency or lower, we may be able to observe a decrease in the number of NPs bound per cell. This could also be the case if NPs were tested on non-activated cells that express lower amounts of ICAM. Furthermore, by decreasing the time of incubation to 30 min vs. 1 h, the number of NPs bound per cell could have also been different for the formulations used, since binding should be faster for NPs bearing higher number of antibody molecules.

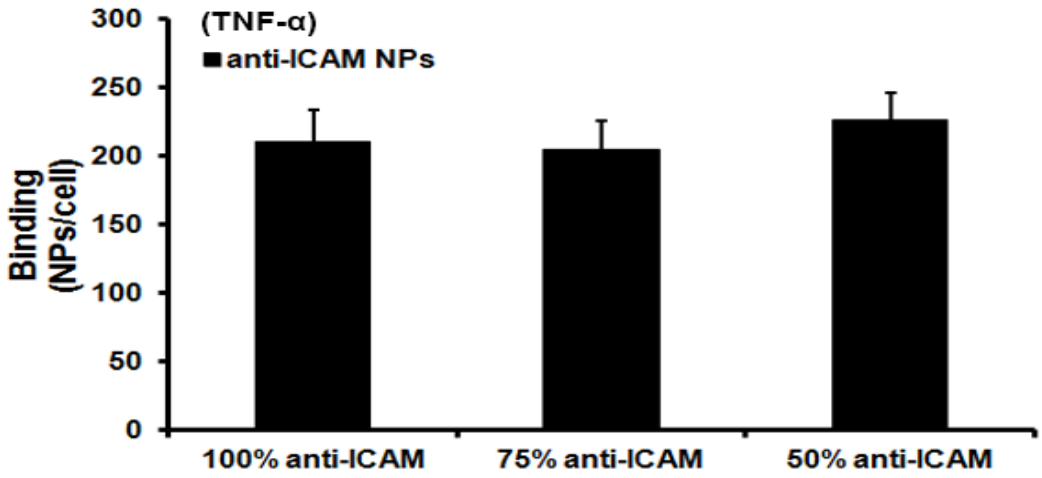

Figure 12. Binding of anti-ICAM NPs with different valencies to TNFα-activated HUVECs. NPs were incubated with cells for 1 h at 37 ^{o}C and analyzed as in Figure 11. Data are mean ± S.E.M.

Finally, we investigated the effect of NP concentration on binding. Cells were TNFα-stimulated and incubated for 1 h at 37 ^{o}C with different concentrations of anti-ICAM PLGA NP at 100%-valency (Figure 13): $2.28x10^{9}$ NPs/μL (standard concentration), $1.14x10^{9}$ NPs/μL (0.5x), and $2.28x10^{8}$ NPs/μL (0.1x). Interestingly, there was a statistically significant decrease on the number of NPs bound per cell at 0.1x concentration over the standard concentration of NPs, from 211±27 to 124±6 NPs/cell. However, in the case of 0.5x concentration there was no effect on binding (218±14 NPs/cell). This verifies the fact that binding of an antibody to its ligand is a concentration dependent event, although the valencies and NP concentration used in the previous experiment (Figure 12) on TNFα-activated cells may be at saturation, which may explain the similar binding obtained for all three conditions. Ultimately, this increase in the number of NPs bound/cell in TNFα-activated cells after increasing the concentration of NPs is in accord with previous studies conducted from our group

using polystyrene NPs [71, 93]. For instance, TNFα-activated HUVECs incubated with a similar standard concentration of 100% targeting valency polystyrene NPs (~220 antibody molecules/NP) at 4 ^{o}C for 1 hr, rendered ~200 NPs bound per cell, similar to PLGA NPs tested in this study, whereas a ~30% decrease in binding was observed in the number of NPs bound per cell when NPs were applied at a concentration 0.1x of the standard value. However, in this study, 100% valency PLGA NPs applied at 0.1x of the standard concentration showed a ~50% decrease on the number of NPs bound per cell [71], which might be due to the higher number of antibody molecules per NPs in this formulation (~310 antibodies/NP) compared to polystyrene NPs, hence PLGA NPs seem more sensitive to this change [71]. Furthermore, in a previous study [71], 100% valency anti-ICAM PLGA NPs that contained surfactant on their surface showed increase specificity over non-targeted counterparts on TNFα-activated HUVECs after 1hr of incubation at 4 ^{o}C, and this increase was similar to the one observed here for our surfactant free PLGA NPs. However, the absolute number of NPs bound per cell for those NPs were ~180 NPs/cell [71] compared to our surfactant free PLGA NPs that was ~220 NPs/cell. Therefore, surfactant free PLGA NPs formulated in this study seem to behave slightly better in terms of the number of antibodies bound per NP at saturation and the number of NPs bound per cell in deceased-like conditions than the polystyrene and PLGA NPs previously used.

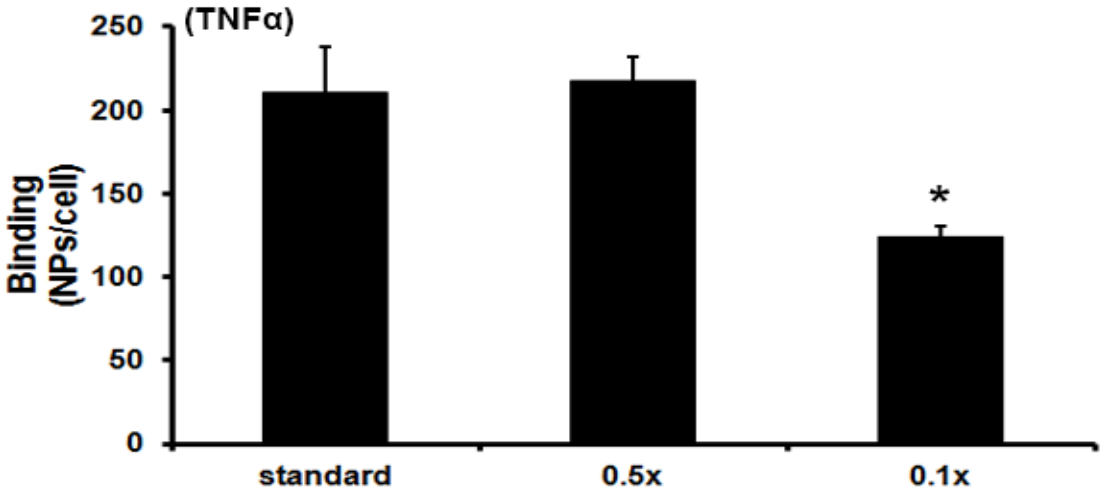

Figure 13. Binding of FITC-labeled, 100%-valency anti-ICAM PLGA NPs to TNFα-activated HUVECs. NPs were incubated with cells for 1 h at 37 ^{o}C at different concentrations. The number of NP bound per cell is shown for concentrations: $2.28x10^{9}$(standard), $1.14x10^{9}$ (0.5x), and $2.28x10^{8}$ (0.1x) NPs/μL. *$p \leq 0.05$, compares the various concentrations to standard concentration of NPs. Data are mean ± S.E.M. ($n \geq 20$ cells).

4.2.3. Internalization of anti-ICAM PLGA NPs into HUVECs

In addition to binding, endocytosis is of major importance since it is one of the parameters that contribute to the transport of the NPs into the cell body, or across cellular barriers to reach further tissues. To determine the internalization efficiency (percentage of NPs internalized by the cells from the total cell-associated NP fraction) of anti-ICAM PLGA NPs by HUVECs, we also used fluorescence microscopy. In this set of experiments we investigated the internalization of NPs in control versus diseased-like conditions (Figure 14a), as well as the effect of antibody density on the internalization efficiency of the NPs by TNFα-activated HUVECs (Figure 14b). In agreement with the fact that more anti-ICAM NPs bound to diseased-like HUVECs as

compared to control cells, more NPs were endocytosed after 1 h incubation at 37 ^{o}C. Specifically, we found 52% internalization for control cells, with a total number of 105 NPs associated per cell and 54±4 NPs internalized/cell. In the case of diseased-like cells, we found that the number of NPs internalized per cell doubled (108±7 NPs/cell). This suggests that anti-ICAM NPs selectively bind and internalize into diseased cells.

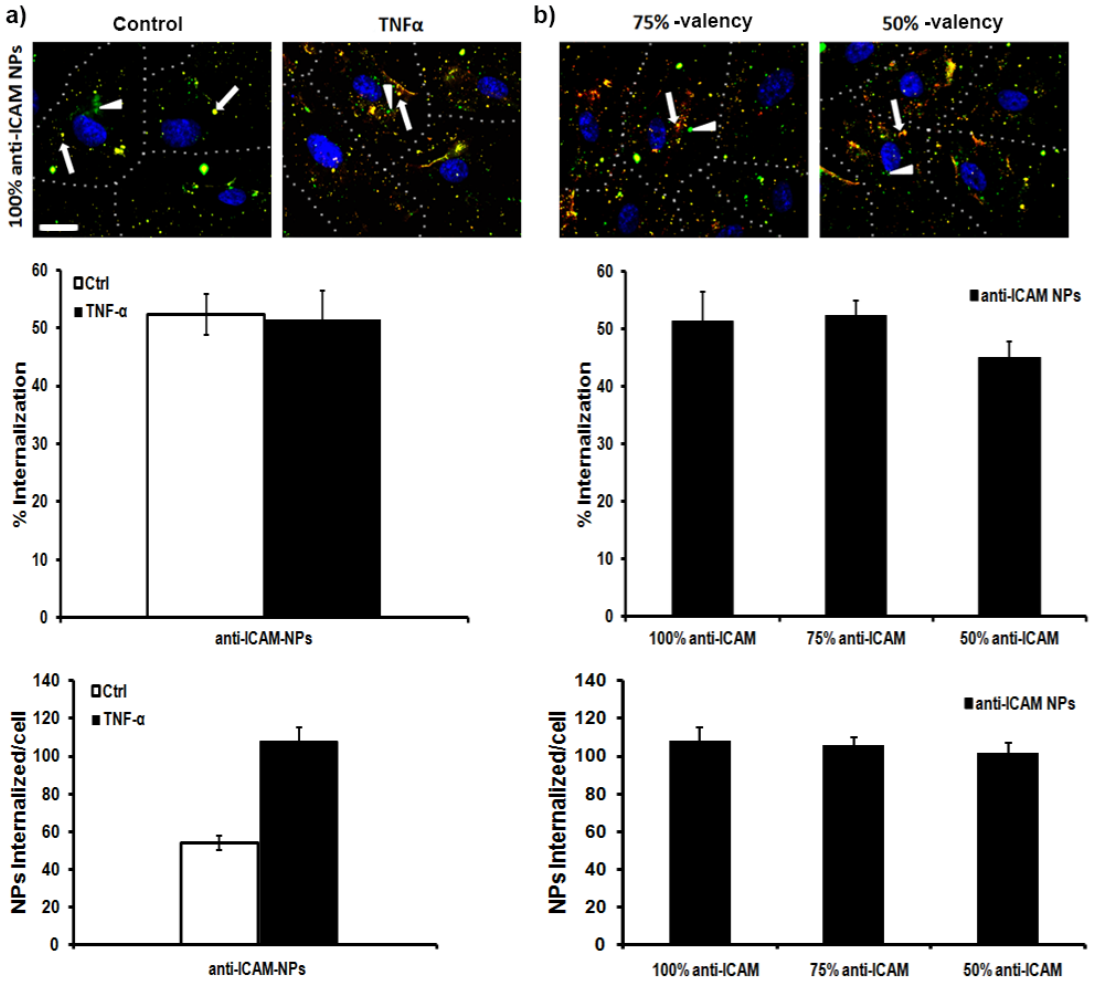

Figure 14. Internalization of anti-ICAM PLGA NPs into HUVECs. Control or TNFα-activated cells were incubated with FITC-labeled anti-ICAM NPs (100% targeting valency) for 1 hour at 37 ^{o}C. Non-bound NPs were then washed and surface bound NPs were stained with Texas Red secondary antibody (red). Fluorescent images were captured and analyzed by microscopy, were green NPs are internalized (arrow heads), whereas yellow NPs (green + red) are surface bound (arrows). (a) Percent internalization and total anti-ICAM NPs internalized by HUVECs, under control or TNFα-stimulated conditions. Scale bar = 10μm. (b) Percent uptake and total anti-ICAM NPs internalized, coated with various antibody densities. Blue = nuclei of the cells. Dashed lines represent the cell borders as observed by phase-contrast. Data are mean ± S.E.M.

As shown in Figure 14a, the percentage of anti-ICAM NPs internalized by the diseased cells was similar between diseased and healthy cells: 52±4% in healthy

versus 51±5% in diseased HUVECs. Interestingly, this result verifies that endocytosis of each anti-ICAM NP via the CAM-pathway is an independent event, not related to the surface density of ICAM-1 nor the number of nanocarriers bound per cell, as previously reported by our group [59, 98]. Furthermore, similar to binding, the percent internalization of anti-ICAM NPs did not change by lowering the number of anti-ICAM molecules present on the surface of the NPs (Figure 14b). Also, the total number of NPs internalized/cell for the three different antibody densities (100%, 75%, and 50%-valency) used in this study was similar: 108±7, 106±4, and 102±5 NPs/cell, respectively. Therefore, anti-ICAM surface densities in the range of 100% to 50%-valencies, do not affect the NP internalization process in activated HUVECs. These results are in accordance with previous data regarding the uptake of anti-ICAM polystyrene NPs [59]. Those previous studies had shown that TNFα had little effect on the mechanism of internalization, since similar results were obtained for the percentage of internalization of anti-ICAM polystyrene NPs in control and diseased-like cells, despite the difference in absolute binding in the absence (~42 NPs/cell) or presence of TNFα (~165 NPs/cell) [59]. Ultimately, surfactant free PLGA NPs formulated in this study showed similar uptake profiles as previously tested polystyrene NPs in control and TNFα-activated cells, although they exhibited slightly higher binding in both control as well as diseased-like conditions, compared to polystyrene NPs. Hence, the results of this experiment supports the potential medical utility of anti-ICAM PLGA NPs in targeting ECs.

4.2.4. Mechanism of endocytosis of anti-ICAM PLGA NPs into HUVECs

As previously reported by our group, binding to ICAM-1 leads to CAM-mediated endocytosis which is not related to any of the common endocytic pathways (e.g. clathrin- and caveolae-mediated pathways) and can provide an avenue of vesicular transport of NPs of various shapes and sizes into or across endothelial cells [44, 52, 75, 99]. When cells were incubated with amiloride, an inhibitor of Na^+/H^+ exchanger involved in CAM-mediated endocytosis, internalization of anti-ICAM PLGA NPs was significantly reduced by 49.9±10.9%. On the other hand, endocytosis in cells treated with filipin, which inhibits caveolae-mediated endocytosis, or MDC, which inhibits clathrin-mediated endocytosis, was not affected (116.3±13.3% and 103.1±14.2%, of control respectively), as expected (Figure 15). The result of this experiment has proved for the first time that anti-ICAM PLGA NPs uptake is mediated by the CAM pathway, as opposed to clathrin- and caveolae-dependent mechanisms, as previously observed for anti-ICAM polystyrene NPs [59]. Similar to the results of this study, inhibition of the caveolae- or clathrin-mediated endocytosis, by the addition of filipin and MDC respectively did not affect the percent uptake of anti-ICAM polystyrene NPs by HUVECs [59]. However, when amiloride was used as an inhibitor there was a ~50% decrease in the uptake of these particles observe in previous studies, similar to that of the PLGA NPs used in this study [59]. Hence, these PLGA NPs may prove to be beneficial in assisting delivery of therapeutics via

this non-classical route of endocytosis and show that FITC labeling and absence of surfactant in this formulation does not affect these aspects.

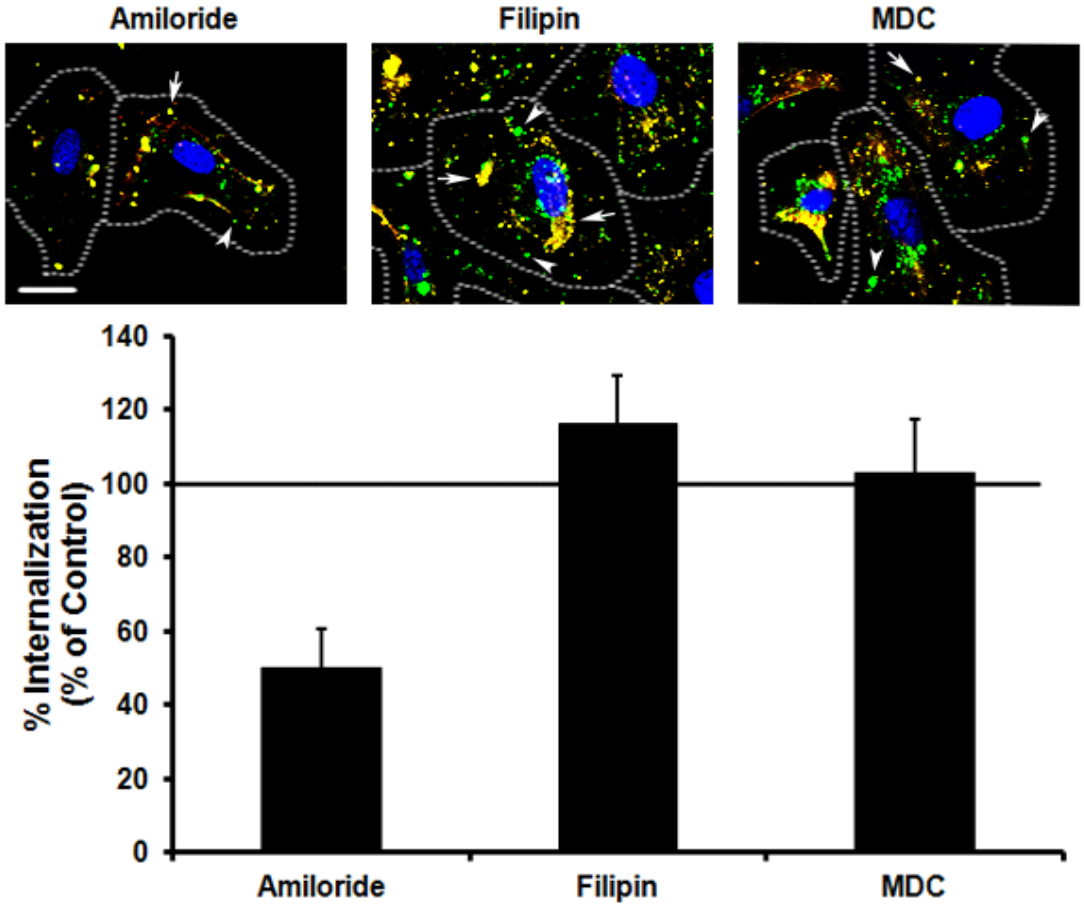

Figure 15. Endocytosis mechanism of anti-ICAM PLGA NPs into HUVECs. TNFα-stimulated HUVECs were incubated with 100% anti-ICAM NPs for 1 h at 37 ^{o}C in absence (control) or in presence of either amiloride (CAM-mediated endocytosis inhibitor), filipin (caveolae-mediated endocytosis inhibitor), or MDC (clathrin-mediated endocytosis inhibitor). Non-bound NPs were then washed and surface bound NPs were stained with Texas Red secondary antibody (red). Fluorescent images were captured and analyzed by microscopy, were green NPs are internalized (arrows), whereas yellow NPs (green + red) are surface bound (arrow heads). Percent internalization relative to control cells is shown. Blue = nuclei of the cells. Dashed lines represent the cell borders as observed by phase-contrast. *$p \leq 0.05$, compares the various inhibitors to control cells. Data are mean ± S.E.M. ($n \geq 20$ cells).

4.2.5. Lysosomal trafficking of anti-ICAM PLGA NPs in HUVECs

Previous works have shown that CAM-mediated endocytosis results in anti-ICAM NP trafficking to lysosomes [59]. This, makes CAM-mediated transport a very prominent route for delivery of therapeutics to lysosomes, such as enzymes for the treatment of lysosomal storage disorders (LSDs), which our group is pursuing [52]. In this study, we aimed to evaluate whether anti-ICAM PLGA NPs can be transported to lysosomes similarly to polystyrene NPs, previously tested by our group. We assessed this by first labeling lysosomes with TexasRed dextran, as previously described [59] and following the FITC-labeled anti-ICAM PLGA NPs over time via fluorescence microscopy (Figure 16).

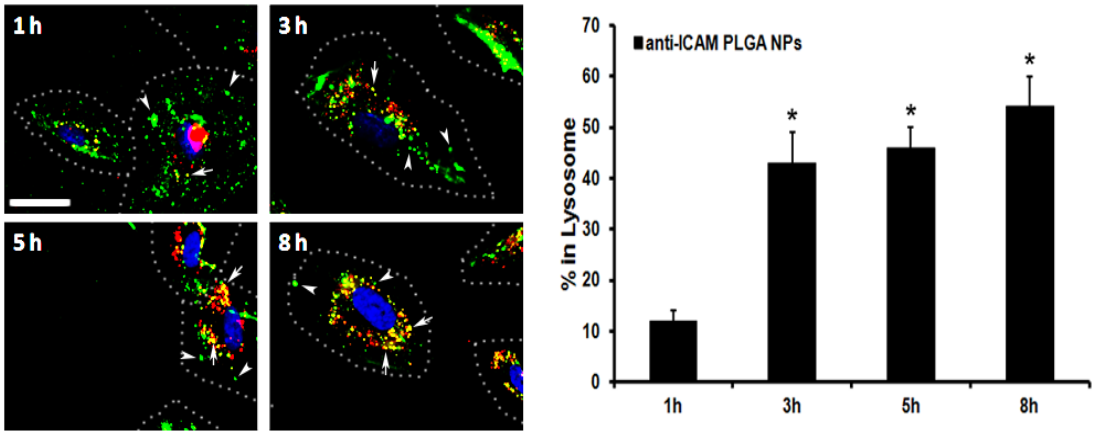

Figure 16. Lysosomal trafficking of anti-ICAM PLGA NPs. TNFα-activated HUVECs were pre-treated with TexasRed dextran to label lysosomes (red). Then, cells were incubated with NPs for 1 h at 37 ^{o}C. Cells were washed to remove unbound NPs, and the bound fraction was followed over time via fluorescence microscopy. Green colored objects represent NPs associated to the cells (arrows), but not in lysosomes, while yellow (green + red) color objects represent NPs colocalized with lysosomes (arrow heads). Dashed lines represent the cell borders as observed by phase-contrast. *p≤0.05, compares to 1 h time point. Scale bar = 10 μm. Data are mean ± S.E.M.

Our results showed that by 3 h there is a statistically significant increase in the number of NPs colocalized with lysosomes in TNFα-stimulated HUVECs (12±2% at 1 h versus 43±6% at 3 h). Interestingly, there was no significant changes in the percent lysosomal colocalization between 3 and 8 h (43±6%, 46±4%, and 54±6% localization at 3, 5, and 8 h, respectively). This indicates that the amount of NPs that traffic to lysosomes reached a plateau by 3 h and that the rest of NPs associated to cells remain either on the cell surface or in endosomes. Ultimately, if we calculate the % lysosomal colocalization by the number of internalized NPs instead of the total number of NPs associated to the cells the values for 1, 3, 5, and 8 h change to 23%, 58%, 66%, and 79%, respectively.

Previous work with polystyrene anti-ICAM NPs had shown a similar trend. However, polystyrene NPs localized to lysosomes at a higher efficiency: ~75% by 3 h [52], which perhaps is due to the influence of the NP material on the trafficking efficacy to this organelle. Although polystyrene NPs trafficked faster to lysosomes, PLGA NPs achieved similar accumulation (79% of the internalized NPs) after 8 h. This indicates that PLGA NPs can still efficiently traffic to this cell compartment and reach similar value at saturation as compared to polystyrene NPs, but at a slower pace or kinetics. Therefore, anti-ICAM PLGA NPs could be used to deliver therapeutics, such as enzymes to lysosomes to effectively treat LSDs (e.g. delivery of ASM required for types A and B Niemann-Pick disease).

4.3. Biodistribution of ICAM-1-targeted PLGA NPs

4.3.1. Introduction

Intravenously injected therapeutics will first encounter endothelial cells of the vasculature as the first layer of cells that must be targeted in order to penetrate through and reach the tissue of interest in the parenchyma. In the case of therapeutic agents administrated free in solution, or non-targeted NPs, there is suboptimal distribution of the therapeutic cargo to the tissues of interest, since they cannot escape from the circulation while accumulating into clearance organs (e.g. kidneys, liver, spleen) [51-53]. Therefore, drug carriers targeted to the endothelium via ICAM-1, which is abundant on their surface, seems to be a promising strategy. Previous work using anti-ICAM polystyrene and PLGA NPs revealed that targeted NPs can selectively bind to organs with dense vasculature (e.g. lungs), which have a high surface area of ECs that express ICAM-1. The circulation and biodistribution of these ICAM-targeted NPs was significantly different than that of the non-targeted counterparts [44, 71, 75, 85, 86, 93]. In this study our aim is to assess whether anti-ICAM PLGA NPs share the same fate and can successfully target ECs of the vasculature after intravenous administration in wild type mice. Furthermore, we evaluated the effect of different antibody valencies on the biodistribution profile of the anti-ICAM NPs to achieve controlled in vivo endothelial targeting.

4.3.2. Biodistribution of anti-ICAM PLGA NPs in mice

To confirm and quantify in vivo targeting by anti-ICAM PLGA NPs, we injected intravenously PLGA NPs coated with different antibody densities and we compared the biodistribution results to those of control non-specific IgG coated counterparts. Results demonstrate that anti-ICAM PLGA NPs with 100%, and 50%-valency get immediately cleared from the circulation (~50% removal within the first min) while those with 12.5%-valency remain in the circulation at the same extent as the control-IgG NPs, even after 30 min post injection (~13% ID in blood) (Figure 17a). Total liver, lungs, and spleen accumulation of NPs with 100% and 50%-valency was similar: 37.40±1.83, 140.20±20.89, and 40.54±3.30 % ID for 100% valency and 38.32±3.58, 159.82±20.51, and 42.32±5.06 %ID for 50%-valency, respectively (Figure 17b). The accumulation of 25% and 12.5%-valency NPs in the lungs was lower, indicating that the targeting efficiency of the particles is critically affected by the number of antibodies on the NP surface, particularly in the case of 12.5%-valency, were the accumulation in lungs was 29.02±2.62 %ID. Also, for the low valency NPs (25%- and 12.5%-valency) there was an increase in the accumulation in the liver and spleen (clearance organs). Hence, lower targeting potential results in greater clearance by these organs, as expected.

Furthermore, to account for the different circulation of each one of these formulations, the localization ratio (LR) was calculated (ratio of %ID/g in tissue versus %ID/g in blood; Figure 17c). As expected, the anti-ICAM PLGA NPs with

100%, 50%, and 25%-valency showed high LR in organs with dense vasculature, like the lungs (~70, ~85, and ~35 LR, respectively) compared to the 12.5%-valency NPs that had similar biodistribution to the non-targeted IgG counterparts (LR ~5 and ~3, respectively). Then, by dividing the LR of anti-ICAM PLGA NPs over that of control IgG NPs, the specificity index (SI) was determined, defining the specific enhancement provided by the ICAM-1-targeting (Figure 17d). NPs with 12.5%-valency bound with low specificity to the lungs (SI = 2.4±0.1), while increasing the targeting valency to 25% and 50% increased SI to 11.7±0.5 and 30.3±1.9, respectively. It appears 50% valency to be optimal, since 100% valency showed a bit lower SI as compared to 50% valency (SI = 24.9±1.1). This may be due to the level of expression of ICAM on the lung endothelium surface, where 50% valency may engage receptors more efficiently than 100% valency. Data for other organs is shown in Table 3.

Previous studies with 100%-valency anti-ICAM polystyrene NPs in mice have shown a similar biodistribution profile and pulmonary targeting compared to the PLGA NPs tested in this study [71]. For instance, the total amount of anti-ICAM polystyrene NPs in circulation 1 min and 15 min after injection was ~5 and ~3.5, respectively, similar to that of PLGA NPs used in this work (~7 and ~3 % ID at 1 and 15 min, respectively) [71]. Furthermore, ~180% ID/g accumulated in the lungs in the case of 100%-valency anti-ICAM polystyrene NPs, similar to the PLGA NPs (~150% ID/g). These results prove that both anti-ICAM polystyrene and PLGA NPs disappear rapidly from the circulation and specifically target the lungs versus the control IgG

counterparts. In addition, previously tested anti-ICAM PLGA NPs that contained surfactant had also shown to efficiently and specifically accumulate in the lungs (~170% ID/g and ~40 SI) similarly to the surfactant free PLGA NPs used in this study (~160% ID/g and ~30 SI). Therefore, in this study we were able to develop PLGA NPs with a simpler formulation, by eliminating surfactant from the NP structure, which showed similar biodistribution profile and lung specificity to previously tested polystyrene and PLGA NPs. Hence, these NPs can potentially be used to enhance the delivery of therapeutics for the treatment of various diseases, such as ASM-deficient Niemann-Pick disease.

Table 3. Biodistribution and specificity of antibody-coated NPs injected in mice.

NPs	Brain		Heart		Kidney	
	LR	SI	LR	SI	LR	SI
– IgG NCs	0.06±0.001	-	0.4±0.03	-	0.6±0.07	-
– Anti-ICAM NCs						
100%-valency	0.06±0.01	1.03±0.1	0.55±0.06	1.3±0.03	2.1±0.3	3.4±0.2
50%-valency	0.07±0.001	1.1±0.02	0.58±0.25	1.4±0.02	2.4±0.3	3.9±0.3
25%-valency	0.04±0.006	0.6±0.2	0.4±0.03	1.03±0.1	1.1±0.08	1.8±0.8
12.5%-valency	0.03±0.001	0.5±0.01	0.2±0.01	0.5±0.01	0.4±0.01	0.7±0.1

NPs	Liver		Lungs		Spleen	
– IgG NCs	LR	SI	LR	SI	LR	SI
– Anti-ICAM NCs	10.6±0.4	-	2.7±0.1	-	16±0.7	-
100%-valency						
50%-valency	18±1.11	1.7±0.04	68±9.7	24±1.1	19±1.1	1.8±0.05
25%-valency	20±2.35	1.9±0.02	83±10.5	30±1.9	21±1.3	1.3±0.02
12.5%-valency	15±1.17	1.4±0.02	32±1.2	11±0.4	23±1.8	1.4±0.01
	8.9±0.9	0.8±0.03	6.6±0.05	2.3±0.1	11.7±1.09	0.7±0.03

Data are Mean ± S.E.M. Ab = antibody; NPs = nanoparticles; LR = localization ratio;
SI = specificity index reported as LR ratio vs. control non-targeted counterparts (IgG NCs).

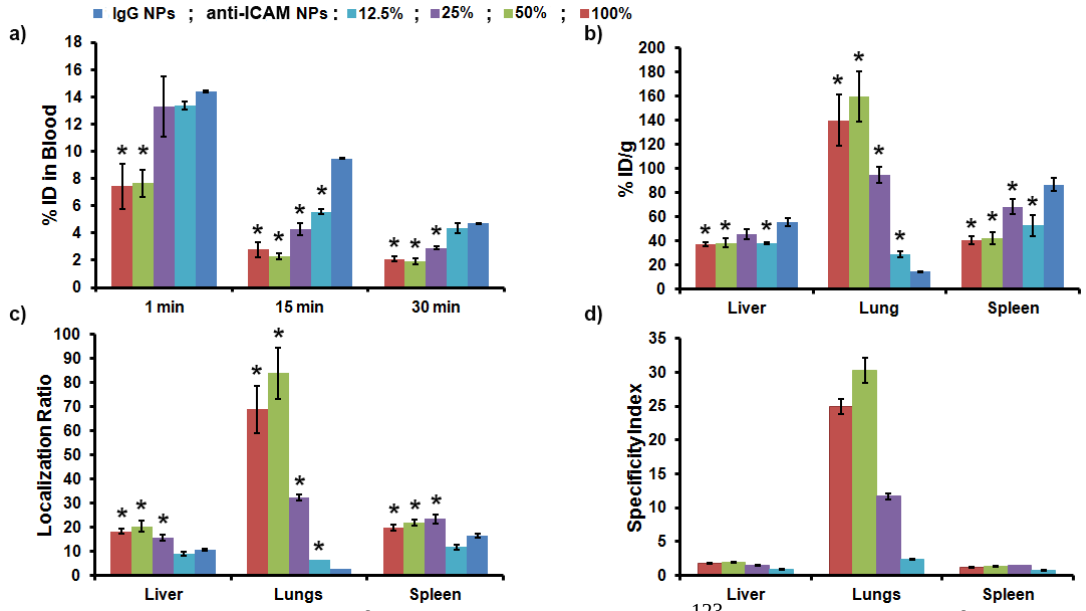

Figure 17. Biodistribution of anti-ICAM PLGA NPs. ^{123}I-labeld non-specific IgG was used to trace NPs in the body. Mice were injected with either control IgG PLGA NPs or anti-ICAM PLGA NPs: 100%, 50%, 25%, or 12.5%-valency. Blood was collected at 1, 15, or 30 min post injection, and organs were collected 30 minutes post injection to measure ^{125}I-antibody using a gamma counter. (a) Percent ID in blood represents the total amount of NPs traced in blood samples. (b) Percent ID/g describes the amount of enzyme traced in each organ normalized by the organs weight. (c) The LR represent the normalized organ accumulation (%ID/g) to the free circulating amount in the blood and represents more accurately the NC retention in the tissue versus that in the blood. (d) The specificity index represents the ratio of the LR between the targeted and the non-targeted NPs. *p≤0.05, compares control-IgG NPs to rest. Data shown are means ± S.E.M.

Section 5: Conclusion and Future Directions

In this study, we formulated solid PLGA NPs by slightly modifying the nanoprecipitation technique to avoid the use of surfactants. Surfactants are commonly used to stabilize the nano-colloidal suspension by creating a highly hydrophilic NP surface and by steric repulsion. However, surfactants are neither FDA approved nor

biodegradable, and can potentially increase toxic side effects [88]. The nanoparticles produced in this study have an average size of 166 nm in diameter. They are spherical, and very monodisperse, with a polydispersity index of 0.065. Also, the nano-colloidal suspension remains stable, even without the presence of surfactants, due the highly negatively charged surface of the particles (zeta potential = -59 mV) and the effect of electrostatic repulsive interactions. Another important advantage of these surfactant-free nanoparticles is their coating ability with antibodies via simple protein adsorption. Therefore, no antibody conjugation reagents are required minimizing thus the risk of crosslinking the nanoparticles, or loosing antibody orientation and targetability [55].

Furthermore, we were able to formulate FITC-labeled PLGA NPs using the same formulation protocol by just adding 5% wt/wt fluorescein in the organic phase. These fluorescently labeled NPs were formulated to be used in cell culture experiments to study the interactoins between anti-ICAM PLGA NPS and HUVECs using fluorescent microscopy. The FITC-loaded NPs showed similar characteristics with the non loaded NPs, but they were slightly larger in size (186 nm in diameter), probably due to the incorporation of the FITC dye which was physically entrapped in the polymer matrix of the NPs [100]. The nanoparticle stability studies revealed that both the non-labeled and FITC-labeled PLGA NPs remain stable in DI water solution, at 4 ^{o}C for at least one month. In addition, both formulations demonstrated good coating efficiencies with antibodies (anti-ICAM or non-specific IgG) and adequate stability of the coat in storage conditions. Moreover, fluorescence intensity

experiments in this study revealed that FITC-labeled NPs lose their fluorescence at pH 4.5, but this effect is reversible when they are transferred back to physiological pH environment (pH of 7.4). This result suggests that in fixed cells, where the pH environment in every compartment of the cell is neutralized, including that of the lysosomes, FITC-labeled NPs regain their fluorescence and can be visualized by fluorescence microscopy.

To complete the characterization of these NPs we studied their degradation profile at 37 ^{o}C in PBS and pH 7.4 or pH 4.5 (to mimic the low pH in the lysosomes). The degradation of PLGA occurs by a bulk erosion mechanism where the ester bonds in the polymer backbone are cleaved by hydrolysis [31, 101]. Initially, there is a decrease in the molecular weight of the polymer without any actual loss of polymer mass, due to random cleavage of the polymer's ester bonds [102]. Then, the acidic microenvironment formed from the initial random hydrolysis of the ester bonds results to further degradation and rapid loss of polymer mass [102]. This acidic microenvironment formed in the core of the NP has an autocatalytic effect in the hydrolysis of the polymer on the surrounding matrix, which leads to higher degradation rates inside the NP than on its surface [101]. Finally, the soluble oligomers created so far in the degradation process are further fragmented to soluble monomers and the NP structure starts altering, resulting in a complete solubilization of the polymer [101]. In this study we followed the decrease of the molecular weight of the polymer over time, along with its result in the structure of the NPs (size, PDI, and FITC release from the NPs). This behavior is validated by our degradation

studies, since the Mw of PLGA decreased from 23 kDa to ~16 kDa after incubation at pH 4.5 (non-coated and IgG-coated NPs), but the count rate and the size of the NPs did not change. Also, there was no significant release of FITC from the NPs until the second day of incubation. However, we can observe a rapid drop in the copolymers Mw from day 7 to day 14 accompanied by a drop in the count rate, which indicates loss of NPs (either due to aggregation and NP precipitation, or due to NP solubilization). This is an indicative of the autocatalytic effect in the polymer's hydrolysis, which accelerates the degradation of the copolymer and leads to higher degradation rate versus that of the first few days. Moreover, the increase of FITC release from the NPs after the second day under all conditions supports the fact that degradation of PLGA is a bulk erosion mechanism which is slow in the beginning, while becomes faster after a few days (2 to 7 days) resulting to high degradation rates in the core of the NPs. This eventually leads to complete solubilization of the NPs which probably starts at day 14 of incubation at 4.5 pH (37 ^{o}C), where the Mw of the polymer is already one third of its initial value and at the same time there is a decrease in the number of counts and a high percent of free FITC in the NP solution. These results validate the fact that PLGA NPs can potentially degrade in the cell after reaching the desired tissues and release their cargo slowly until they are fully degraded and digested from the body.

To address whether anti-ICAM PLGA NPs can target and bind to endothelium we examined in a cell culture model the interactions between these particles and HUVECs. The binding efficiency of ICAM-1 targeted NPs was significantly higher

than that of control (non-targeted) NPs, and it was further increased in the case of diseased cells, where ICAM-1 is known to be overexpressed [61]. This behavior of anti-ICAM PLGA NPs is the same with that of model polystyrene NPs or PLGA targeted to ICAM-1, that were already tested by our group [59, 71]. Also, the binding efficiency of the particles was not affected by lowering the density of anti-ICAM on their surface. Previously published data have shown that NP with lower antibody densities bind at a lower extent than those with higher antibody densities [71]. However, in this study all the different antibody densities used led to a similar number of NPs bound per cell. This is probably because all the NP formulations used carried more than ~150 antibodies/NP which is an antibody density close to saturation according to the literature [71]. This means that anti-ICAM PLGA NPs with lower than 50%-valency could potentially result to less binding after 1 h of incubation with cells. Furthermore, the antibody densities used in this study may have different binding kinetics. Incubation of these NPs with cells for less than 1 h could result in less binding of the lower valency NPs (50%-valency) compared to the higher valency ones (75% and 100%-valency). Finally, we used diseased-like cells that overexpress ICAM-1 and that is a parameter that could affect the binding of the lower density NPs [93]. In the case of healthy ECs, where ICAM-1 is not upregulated, we might have seen differences in the binding efficiency of NPs at 50%, 75%, or 100%-valency. Next, we tested anti-ICAM PLGA NP with 100%-valency at different concentrations. Concentration of NPs is another parameter that has been shown to affect binding of NPs to ECs [93]. Our results were similar to previous studies, since

lower NP concentrations exhibited significantly lower binding, validating the fact that concentration of NPs has also an important role on their binding efficiency.

Additionally, control and diseased-like ECs demonstrated the ability to internalize, and traffic anti-ICAM PLGA NPs to lysosomes via CAM-mediated endocytosis. This result is in accordance with previous work conducted from our research group where model polystyrene anti-ICAM NPs have shown enhanced binding, internalization, and lysosomal trafficking through the CAM-pathway [64]. While this was observed with model polystyrene NPs, the FITC-labeled PLGA NPs synthesized in this study have enabled a detailed examination of the parameters that affect binding, internalization, and intracellular transport of anti-ICAM PLGA NPs by ECs in cell cultures. The results demonstrated that ICAM-1-targeted PLGA NPs behave similarly to the polystyrene counterparts, and along with the degradation experiments conducted they can provide a promising alternative for future clinical studies.

Ultimately, we investigated the biodistribution of anti-ICAM PLGA NPs in vivo, where ICAM-1-targeted NPs showed enhanced delivery over non-targeted control NPs to the spleen, the liver, and particularly the lungs. Also, these NPs were completely cleared from the circulation after 15 min post-injection, which further validates their enhanced targeting ability. Once again, these results resemble the findings from previous studies were ICAM-1-targeted model polystyrene NPs and PLGA NPs have shown to specifically accumulate to the lungs, although they also accumulate in the spleen and liver [71]. This result is appropriate and valuable for

delivery of lysosomal enzymes, where all these organs are targets for intervention. In addition, we studied the effects of antibody density on the biodistribution profile of NPs. Similarly to the cell culture results, anti-ICAM PLGA NPs with lower antibody densities, 50% to 100% anti-ICAM, had showed similar binding efficiencies and biodistribution profiles. Furthermore, NPs coated with even lower antibody densities, such as 25%-valency, can still target specifically the lungs, but they need more time to leave the circulation. Finally, 12.5%-valency NPs do not leave the circulation completely (4.37±0.36 % ID in blood; similar to IgG-NPs after 30min post-injection), although their specificity index in the lungs is still above one, indicating specific targeting to this organ.

Through this study, advances toward a better understanding of interactions between ECs and ICAM-1-targeted PLGA NPs has been achieved. Also, the in vitro degradation studies of these NPs, along with the investigation of their biodistribution after intravenous administration in mice have significantly enhance previous knowledge. However, the work presented here is a proof-of-concept model and additional work still needs to be done to advance anti-ICAM PLGA NPs toward pre-clinical trials. Firstly, future studies should focus on the degradation of the NPs after internalization by the cells, both in culture and in vivo. This study proved that anti-ICAM PLGA NPs accumulate in the lysosomes of ECs in culture and the lungs of mice in vivo. Therefore, it might be worth to investigate the degradation of the NPs in these two specific environments. Furthermore, potential therapeutics (e.g. enzymes) can be loaded on the surface of the NPs or be encapsulated into the NPs to study

delivery of those therapeutics to certain cell compartments (e.g. lysosomes) or tissues (e.g. lungs). Since encapsulation of the therapeutic cargo can potentially protect and control its release upon degradation, it would be beneficial to study the activity of the delivered enzyme in the case of surface-bound versus encapsulated formulations. In addition, these NPs can be further tested in other cell types (e.g., astrocytes, brain vascular pericytes, neurons, and gastrointestinal epithelial cells). Ultimately, toxicity studies in cell cultures as well as in mice (particularly at the organs of accumulation) would help guide this drug targeting strategy one step closer to the clinics.

All in all, this study has shown the potential of ICAM-1-targeted PLGA NPs as a drug delivery system that can specifically target diseased ECs. This targeted NP model will have to be optimized further for its future potential use in clinical treatments (e.g. LSDs).

References

[1] Anselmo AC, Mitragotri S. An overview of clinical and commercial impact of drug delivery systems. Journal of controlled release : official journal of the Controlled Release Society 2014;190:15-28.

[2] Mudshinge SR, Deore AB, Patil S, Bhalgat CM. Nanoparticles: Emerging carriers for drug delivery. Saudi pharmaceutical journal : SPJ : the official publication of the Saudi Pharmaceutical Society 2011;19:129-41.

[3] Torchilin VP. Recent advances with liposomes as pharmaceutical carriers. Nature reviews Drug discovery 2005;4:145-60.

[4] Musacchio T, Torchilin VP. Recent developments in lipid-based pharmaceutical nanocarriers. Frontiers in bioscience 2011;16:1388-412.

[5] Gelperina S, Kisich K, Iseman MD, Heifets L. The potential advantages of nanoparticle drug delivery systems in chemotherapy of tuberculosis. American journal of respiratory and critical care medicine 2005;172:1487-90.

[6] Sanvicens N, Marco MP. Multifunctional nanoparticles--properties and prospects for their use in human medicine. Trends in biotechnology 2008;26:425-33.

[7] Alexis F, Pridgen E, Molnar LK, Farokhzad OC. Factors affecting the clearance and biodistribution of polymeric nanoparticles. Molecular pharmaceutics 2008;5:505-15.

[8] Ensign LM, Cone R, Hanes J. Oral drug delivery with polymeric nanoparticles: the gastrointestinal mucus barriers. Advanced drug delivery reviews 2012;64:557-70.

[9] Pack DW, Hoffman AS, Pun S, Stayton PS. Design and development of polymers for gene delivery. Nature reviews Drug discovery 2005;4:581-93.

[10] Lee JS, Green JJ, Love KT, Sunshine J, Langer R, Anderson DG. Gold, poly(beta-amino ester) nanoparticles for small interfering RNA delivery. Nano letters 2009;9:2402-6.

[11] Puri A, Loomis K, Smith B, Lee JH, Yavlovich A, Heldman E, et al. Lipid-based nanoparticles as pharmaceutical drug carriers: from concepts to clinic. Critical reviews in therapeutic drug carrier systems 2009;26:523-80.

[12] Elzoghby AO, Samy WM, Elgindy NA. Protein-based nanocarriers as promising drug and gene delivery systems. Journal of controlled release : official journal of the Controlled Release Society 2012;161:38-49.

[13] Oh M, Mirkin CA. Chemically tailorable colloidal particles from infinite coordination polymers. Nature 2005;438:651-4.

[14] Qi L, Gao X. Emerging application of quantum dots for drug delivery and therapy. Expert opinion on drug delivery 2008;5:263-7.

[15] Croy SR, Kwon GS. Polymeric micelles for drug delivery. Current pharmaceutical design 2006;12:4669-84.

[16] Haley B, Frenkel E. Nanoparticles for drug delivery in cancer treatment. Urologic oncology 2008;26:57-64.

[17] Arayne MS, Sultana N. Porous nanoparticles in drug delivery systems. Pakistan journal of pharmaceutical sciences 2006;19:158-69.

[18] Soppimath KS, Aminabhavi TM, Kulkarni AR, Rudzinski WE. Biodegradable polymeric nanoparticles as drug delivery devices. Journal of controlled release : official journal of the Controlled Release Society 2001;70:1-20.

[19] Danhier F, Ansorena E, Silva JM, Coco R, Le Breton A, Preat V. PLGA-based nanoparticles: an overview of biomedical applications. Journal of controlled release : official journal of the Controlled Release Society 2012;161:505-22.

[20] Muro S. New biotechnological and nanomedicine strategies for treatment of lysosomal storage disorders. Wiley interdisciplinary reviews Nanomedicine and nanobiotechnology 2010;2:189-204.

[21] Wu L, Zhang J, Watanabe W. Physical and chemical stability of drug nanoparticles. Advanced drug delivery reviews 2011;63:456-69.

[22] Dorresteijn R, Ragg R, Rago G, Billecke N, Bonn M, Parekh SH, et al. Biocompatible polylactide-block-polypeptide-block-polylactide nanocarrier. Biomacromolecules 2013;14:1572-7.

[23] Varela MC, Guzman M, Molpeceres J, del Rosario Aberturas M, Rodriguez-Puyol D, Rodriguez-Puyol M. Cyclosporine-loaded polycaprolactone nanoparticles: immunosuppression and nephrotoxicity in rats. European journal of pharmaceutical sciences : official journal of the European Federation for Pharmaceutical Sciences 2001;12:471-8.

[24] Rancan F, Papakostas D, Hadam S, Hackbarth S, Delair T, Primard C, et al. Investigation of polylactic acid (PLA) nanoparticles as drug delivery systems for local dermatotherapy. Pharmaceutical research 2009;26:2027-36.

[25] Bala I, Hariharan S, Kumar MN. PLGA nanoparticles in drug delivery: the state of the art. Critical reviews in therapeutic drug carrier systems 2004;21:387-422.

[26] Pacurari M, Qian Y, Fu W, Schwegler-Berry D, Ding M, Castranova V, et al. Cell permeability, migration, and reactive oxygen species induced by multiwalled carbon nanotubes in human microvascular endothelial cells. Journal of toxicology and environmental health Part A 2012;75:129-47.

[27] Menon JU, Ravikumar P, Pise A, Gyawali D, Hsia CC, Nguyen KT. Polymeric nanoparticles for pulmonary protein and DNA delivery. Acta biomaterialia 2014;10:2643-52.

[28] Chawla JS, Amiji MM. Biodegradable poly(epsilon -caprolactone) nanoparticles for tumor-targeted delivery of tamoxifen. International journal of pharmaceutics 2002;249:127-38.

[29] Li Y, Pei Y, Zhang X, Gu Z, Zhou Z, Yuan W, et al. PEGylated PLGA nanoparticles as protein carriers: synthesis, preparation and biodistribution in rats. Journal of controlled release : official journal of the Controlled Release Society 2001;71:203-11.

[30] Yun X, Maximov VD, Yu J, Zhu H, Vertegel AA, Kindy MS. Nanoparticles for targeted delivery of antioxidant enzymes to the brain after cerebral ischemia and

reperfusion injury. Journal of cerebral blood flow and metabolism : official journal of the International Society of Cerebral Blood Flow and Metabolism 2013;33:583-92.
[31] Makadia HK, Siegel SJ. Poly Lactic-co-Glycolic Acid (PLGA) as Biodegradable Controlled Drug Delivery Carrier. Polymers 2011;3:1377-97.
[32] Kumari A, Yadav SK, Yadav SC. Biodegradable polymeric nanoparticles based drug delivery systems. Colloids and surfaces B, Biointerfaces 2010;75:1-18.
[33] Mundargi RC, Babu VR, Rangaswamy V, Patel P, Aminabhavi TM. Nano/micro technologies for delivering macromolecular therapeutics using poly(D,L-lactide-co-glycolide) and its derivatives. Journal of controlled release : official journal of the Controlled Release Society 2008;125:193-209.
[34] Mora-Huertas CE, Fessi H, Elaissari A. Polymer-based nanocapsules for drug delivery. International journal of pharmaceutics 2010;385:113-42.
[35] Minost A, Delaveau J, Bolzinger MA, Fessi H, Elaissari A. Nanoparticles via nanoprecipitation process. Recent patents on drug delivery & formulation 2012;6:250-8.
[36] Bilati U, Allemann E, Doelker E. Development of a nanoprecipitation method intended for the entrapment of hydrophilic drugs into nanoparticles. European journal of pharmaceutical sciences : official journal of the European Federation for Pharmaceutical Sciences 2005;24:67-75.
[37] Barichello JM, Morishita M, Takayama K, Nagai T. Encapsulation of hydrophilic and lipophilic drugs in PLGA nanoparticles by the nanoprecipitation method. Drug development and industrial pharmacy 1999;25:471-6.
[38] Verderio P, Bonetti P, Colombo M, Pandolfi L, Prosperi D. Intracellular drug release from curcumin-loaded PLGA nanoparticles induces G2/M block in breast cancer cells. Biomacromolecules 2013;14:672-82.
[39] Zidan AS, Rahman Z, Habib MJ, Khan MA. Spectral and spatial characterization of protein loaded PLGA nanoparticles. Journal of pharmaceutical sciences 2010;99:1180-92.

[40] Betancourt T, Brown B, Brannon-Peppas L. Doxorubicin-loaded PLGA nanoparticles by nanoprecipitation: preparation, characterization and in vitro evaluation. Nanomedicine 2007;2:219-32.

[41] Santander-Ortega MJ, Bastos-Gonzalez D, Ortega-Vinuesa JL, Alonso MJ. Insulin-loaded PLGA nanoparticles for oral administration: an in vitro physico-chemical characterization. Journal of biomedical nanotechnology 2009;5:45-53.

[42] Morales-Cruz M, Flores-Fernandez GM, Morales-Cruz M, Orellano EA, Rodriguez-Martinez JA, Ruiz M, et al. Two-step nanoprecipitation for the production of protein-loaded PLGA nanospheres. Results in pharma sciences 2012;2:79-85.

[43] Niu X, Zou W, Liu C, Zhang N, Fu C. Modified nanoprecipitation method to fabricate DNA-loaded PLGA nanoparticles. Drug development and industrial pharmacy 2009;35:1375-83.

[44] Garnacho C, Dhami R, Simone E, Dziubla T, Leferovich J, Schuchman EH, et al. Delivery of acid sphingomyelinase in normal and niemann-pick disease mice using intercellular adhesion molecule-1-targeted polymer nanocarriers. The Journal of pharmacology and experimental therapeutics 2008;325:400-8.

[45] McCall RL, Sirianni RW. PLGA nanoparticles formed by single- or double-emulsion with vitamin E-TPGS. Journal of visualized experiments : JoVE 2013:51015.

[46] Vasir JK, Labhasetwar V. Biodegradable nanoparticles for cytosolic delivery of therapeutics. Advanced drug delivery reviews 2007;59:718-28.

[47] Panyam J, Zhou WZ, Prabha S, Sahoo SK, Labhasetwar V. Rapid endo-lysosomal escape of poly(DL-lactide-co-glycolide) nanoparticles: implications for drug and gene delivery. FASEB journal : official publication of the Federation of American Societies for Experimental Biology 2002;16:1217-26.

[48] Owens DE, 3rd, Peppas NA. Opsonization, biodistribution, and pharmacokinetics of polymeric nanoparticles. International journal of pharmaceutics 2006;307:93-102.

[49] Betancourt T, Byrne JD, Sunaryo N, Crowder SW, Kadapakkam M, Patel S, et al. PEGylation strategies for active targeting of PLA/PLGA nanoparticles. Journal of biomedical materials research Part A 2009;91:263-76.

[50] Foged C, Brodin B, Frokjaer S, Sundblad A. Particle size and surface charge affect particle uptake by human dendritic cells in an in vitro model. International journal of pharmaceutics 2005;298:315-22.

[51] Vasir JK, Labhasetwar V. Quantification of the force of nanoparticle-cell membrane interactions and its influence on intracellular trafficking of nanoparticles. Biomaterials 2008;29:4244-52.

[52] Muro S, Schuchman EH, Muzykantov VR. Lysosomal enzyme delivery by ICAM-1-targeted nanocarriers bypassing glycosylation- and clathrin-dependent endocytosis. Molecular therapy : the journal of the American Society of Gene Therapy 2006;13:135-41.

[53] Karra N, Nassar T, Ripin AN, Schwob O, Borlak J, Benita S. Antibody conjugated PLGA nanoparticles for targeted delivery of paclitaxel palmitate: efficacy and biofate in a lung cancer mouse model. Small 2013;9:4221-36.

[54] Graf N, Bielenberg DR, Kolishetti N, Muus C, Banyard J, Farokhzad OC, et al. alpha(V)beta(3) integrin-targeted PLGA-PEG nanoparticles for enhanced anti-tumor efficacy of a Pt(IV) prodrug. ACS nano 2012;6:4530-9.

[55] Kocbek P, Obermajer N, Cegnar M, Kos J, Kristl J. Targeting cancer cells using PLGA nanoparticles surface modified with monoclonal antibody. Journal of controlled release : official journal of the Controlled Release Society 2007;120:18-26.

[56] Chittasupho C, Xie SX, Baoum A, Yakovleva T, Siahaan TJ, Berkland CJ. ICAM-1 targeting of doxorubicin-loaded PLGA nanoparticles to lung epithelial cells. European journal of pharmaceutical sciences : official journal of the European Federation for Pharmaceutical Sciences 2009;37:141-50.

[57] Torchilin VP, Lukyanov AN. Peptide and protein drug delivery to and into tumors: challenges and solutions. Drug discovery today 2003;8:259-66.

[58] Ding BS, Dziubla T, Shuvaev VV, Muro S, Muzykantov VR. Advanced drug delivery systems that target the vascular endothelium. Molecular interventions 2006;6:98-112.

[59] Muro S, Wiewrodt R, Thomas A, Koniaris L, Albelda SM, Muzykantov VR, et al. A novel endocytic pathway induced by clustering endothelial ICAM-1 or PECAM-1. Journal of cell science 2003;116:1599-609.

[60] Rothlein R, Dustin ML, Marlin SD, Springer TA. A human intercellular adhesion molecule (ICAM-1) distinct from LFA-1. Journal of immunology 1986;137:1270-4.

[61] Hubbard AK, Rothlein R. Intercellular adhesion molecule-1 (ICAM-1) expression and cell signaling cascades. Free radical biology & medicine 2000;28:1379-86.

[62] van de Stolpe A, van der Saag PT. Intercellular adhesion molecule-1. Journal of molecular medicine 1996;74:13-33.

[63] Carpen O, Pallai P, Staunton DE, Springer TA. Association of intercellular adhesion molecule-1 (ICAM-1) with actin-containing cytoskeleton and alpha-actinin. The Journal of cell biology 1992;118:1223-34.

[64] Muro S, Gajewski C, Koval M, Muzykantov VR. ICAM-1 recycling in endothelial cells: a novel pathway for sustained intracellular delivery and prolonged effects of drugs. Blood 2005;105:650-8.

[65] Haug CE, Colvin RB, Delmonico FL, Auchincloss H, Jr., Tolkoff-Rubin N, Preffer FI, et al. A phase I trial of immunosuppression with anti-ICAM-1 (CD54) mAb in renal allograft recipients. Transplantation 1993;55:766-72; discussion 72-3.

[66] Fischer A. Anti-LFA-1 antibody as immunosuppressive reagent in transplantation. Chemical immunology 1991;50:89-97.

[67] Huang YW, Burrows FJ, Vitetta ES. Cytotoxicity of a novel anti-ICAM-1 immunotoxin on human myeloma cell lines. Hybridoma 1993;12:661-75.

[68] Hsu J, Serrano D, Bhowmick T, Kumar K, Shen Y, Kuo YC, et al. Enhanced endothelial delivery and biochemical effects of alpha-galactosidase by ICAM-1-

targeted nanocarriers for Fabry disease. Journal of controlled release : official journal of the Controlled Release Society 2011;149:323-31.

[69] Liu J, Zhang P, Liu P, Zhao Y, Gao S, Tan K, et al. Endothelial adhesion of targeted microbubbles in both small and great vessels using ultrasound radiation force. Molecular imaging 2012;11:58-66.

[70] Muro S, Koval M, Muzykantov V. Endothelial endocytic pathways: gates for vascular drug delivery. Current vascular pharmacology 2004;2:281-99.

[71] Muro S, Dziubla T, Qiu W, Leferovich J, Cui X, Berk E, et al. Endothelial targeting of high-affinity multivalent polymer nanocarriers directed to intercellular adhesion molecule 1. The Journal of pharmacology and experimental therapeutics 2006;317:1161-9.

[72] Hsu J, Rappaport J, Muro S. Specific binding, uptake, and transport of ICAM-1-targeted nanocarriers across endothelial and subendothelial cell components of the blood-brain barrier. Pharmaceutical research 2014;31:1855-66.

[73] Ghaffarian R, Bhowmick T, Muro S. Transport of nanocarriers across gastrointestinal epithelial cells by a new transcellular route induced by targeting ICAM-1. Journal of controlled release : official journal of the Controlled Release Society 2012;163:25-33.

[74] Mane V, Muro S. Biodistribution and endocytosis of ICAM-1-targeting antibodies versus nanocarriers in the gastrointestinal tract in mice. International journal of nanomedicine 2012;7:4223-37.

[75] Muro S, Garnacho C, Champion JA, Leferovich J, Gajewski C, Schuchman EH, et al. Control of endothelial targeting and intracellular delivery of therapeutic enzymes by modulating the size and shape of ICAM-1-targeted carriers. Molecular therapy : the journal of the American Society of Gene Therapy 2008;16:1450-8.

[76] Charoenphol P, Mocherla S, Bouis D, Namdee K, Pinsky DJ, Eniola-Adefeso O. Targeting therapeutics to the vascular wall in atherosclerosis--carrier size matters. Atherosclerosis 2011;217:364-70.

[77] Beck M. New therapeutic options for lysosomal storage disorders: enzyme replacement, small molecules and gene therapy. Human genetics 2007;121:1-22.

[78] Muro S. Strategies for Delivery of Therapeutics into the Central Nervous System for Treatment of Lysosomal Storage Disorders. Drug delivery and translational research 2012;2:169-86.

[79] Romano PS, Lopez AC, Mariani ML, Sartor T, Belmonte SA, Sosa MA. Expression and binding properties of the two mannose-6-phosphate receptors differ during perinatal development in rat liver. Biochemical and biophysical research communications 2002;295:1000-6.

[80] Rappaport J, Garnacho C, Muro S. Clathrin-mediated endocytosis is impaired in type A-B Niemann-Pick disease model cells and can be restored by ICAM-1-mediated enzyme replacement. Molecular pharmaceutics 2014;11:2887-95.

[81] Nobs L, Buchegger F, Gurny R, Allemann E. Current methods for attaching targeting ligands to liposomes and nanoparticles. Journal of pharmaceutical sciences 2004;93:1980-92.

[82] Ezpeleta I, Arangoa MA, Irache JM, Stainmesse S, Chabenat C, Popineau Y, et al. Preparation of Ulex europaeus lectin-gliadin nanoparticle conjugates and their interaction with gastrointestinal mucus. International journal of pharmaceutics 1999;191:25-32.

[83] Irache JM, Durrer C, Duchene D, Ponchel G. Preparation and characterization of lectin-latex conjugates for specific bioadhesion. Biomaterials 1994;15:899-904.

[84] Zhang N, Chittasupho C, Duangrat C, Siahaan TJ, Berkland C. PLGA nanoparticle--peptide conjugate effectively targets intercellular cell-adhesion molecule-1. Bioconjugate chemistry 2008;19:145-52.

[85] Hsu J, Northrup L, Bhowmick T, Muro S. Enhanced delivery of alpha-glucosidase for Pompe disease by ICAM-1-targeted nanocarriers: comparative performance of a strategy for three distinct lysosomal storage disorders. Nanomedicine 2012;8:731-9.

[86] Hsu J, Bhowmick T, Burks SR, Kao JP, Muro S. Enhancing biodistribution of therapeutic enzymes in vivo by modulating surface coating and concentration of ICAM-1-targeted nanocarriers. Journal of biomedical nanotechnology 2014;10:345-54.

[87] Muro S, Cui X, Gajewski C, Murciano JC, Muzykantov VR, Koval M. Slow intracellular trafficking of catalase nanoparticles targeted to ICAM-1 protects endothelial cells from oxidative stress. American journal of physiology Cell physiology 2003;285:C1339-47.

[88] Vaughan M, van Egmond R. The use of the zebrafish (Danio rerio) embryo for the acute toxicity testing of surfactants, as a possible alternative to the acute fish test. Alternatives to laboratory animals : ATLA 2010;38:231-8.

[89] Chen YP, Chen CT, Hung Y, Chou CM, Liu TP, Liang MR, et al. A new strategy for intracellular delivery of enzyme using mesoporous silica nanoparticles: superoxide dismutase. Journal of the American Chemical Society 2013;135:1516-23.

[90] Muller RH, Keck CM. Challenges and solutions for the delivery of biotech drugs--a review of drug nanocrystal technology and lipid nanoparticles. Journal of biotechnology 2004;113:151-70.

[91] Giteau A, Venier-Julienne MC, Marchal S, Courthaudon JL, Sergent M, Montero-Menei C, et al. Reversible protein precipitation to ensure stability during encapsulation within PLGA microspheres. European journal of pharmaceutics and biopharmaceutics : official journal of Arbeitsgemeinschaft fur Pharmazeutische Verfahrenstechnik eV 2008;70:127-36.

[92] Liu C, Yu W, Chen Z, Zhang J, Zhang N. cNGR conjugated poly(lactic acid)-poly(ethylene glycol) nanoparticles for targeted gene delivery. Journal of controlled release : official journal of the Controlled Release Society 2011;152 Suppl 1:e155-7.

[93] Calderon AJ, Bhowmick T, Leferovich J, Burman B, Pichette B, Muzykantov V, et al. Optimizing endothelial targeting by modulating the antibody density and particle concentration of anti-ICAM coated carriers. Journal of controlled release : official journal of the Controlled Release Society 2011;150:37-44.

[94] Mohammad AK, Reineke JJ. Quantitative detection of PLGA nanoparticle degradation in tissues following intravenous administration. Molecular pharmaceutics 2013;10:2183-9.

[95] Dailey LA, Kleemann E, Wittmar M, Gessler T, Schmehl T, Roberts C, et al. Surfactant-free, biodegradable nanoparticles for aerosol therapy based on the branched polyesters, DEAPA-PVAL-g-PLGA. Pharmaceutical research 2003;20:2011-20.

[96] Muzykantov VR. Biomedical aspects of targeted delivery of drugs to pulmonary endothelium. Expert opinion on drug delivery 2005;2:909-26.

[97] Muro S, Muzykantov VR. Targeting of antioxidant and anti-thrombotic drugs to endothelial cell adhesion molecules. Current pharmaceutical design 2005;11:2383-401.

[98] Papademetriou J, Garnacho C, Serrano D, Bhowmick T, Schuchman EH, Muro S. Comparative binding, endocytosis, and biodistribution of antibodies and antibody-coated carriers for targeted delivery of lysosomal enzymes to ICAM-1 versus transferrin receptor. Journal of inherited metabolic disease 2013;36:467-77.

[99] Ansar M, Serrano D, Papademetriou I, Bhowmick TK, Muro S. Biological functionalization of drug delivery carriers to bypass size restrictions of receptor-mediated endocytosis independently from receptor targeting. ACS nano 2013;7:10597-611.

[100] Chang J, Jallouli Y, Kroubi M, Yuan XB, Feng W, Kang CS, et al. Characterization of endocytosis of transferrin-coated PLGA nanoparticles by the blood-brain barrier. International journal of pharmaceutics 2009;379:285-92.

[101] Park TG. Degradation of poly(lactic-co-glycolic acid) microspheres: effect of copolymer composition. Biomaterials 1995;16:1123-30.

[102] Pitt CG, Gratzl MM, Kimmel GL, Surles J, Schindler A. Aliphatic polyesters II. The degradation of poly (DL-lactide), poly (epsilon-caprolactone), and their copolymers in vivo. Biomaterials 1981;2:215-20.